Partitioning of ocean and land uptake of CO_2 as inferred by $\delta^{13}C$ measurements from the NOAA Climate Monitoring and Diagnostics Laboratory Global Air Sampling Network

Philippe Ciais,[1,2,3] Pieter P. Tans,[2] James W. C. White,[1,4] Michael Trolier,[1,2]
Roger J. Francey,[5] Joe A. Berry,[6] David R. Randall,[7]
Piers J. Sellers,[8] James G. Collatz,[8] and David S. Schimel[3]

Abstract. Using $\delta^{13}C$ measurements in atmospheric CO_2 from a cooperative global air sampling network, we determined the partitioning of the net uptake of CO_2 between ocean and land as a function of latitude and time. The majority of $\delta^{13}C$ measurements were made at the Institute of Arctic and Alpine Research (INSTAAR) of the University of Colorado. The network included 40 sites in 1992 and constitutes the most extensive data set available. We perform an inverse deconvolution of both CO_2 and $\delta^{13}C$ observations, using a two-dimensional model of atmospheric transport. New features of the method include a detailed calculation of the isotopic disequilibrium of the terrestrial biosphere from global runs of the CENTURY soil model. Also, the discrimination against ^{13}C by plant photosynthesis, as a function of latitude and time, is calculated from global runs of the SiB biosphere model. Uncertainty due to the longitudinal structure of the data, which is not represented by the model, is studied through a bootstrap analysis by adding and omitting measurement sites. The resulting error estimates for our inferred sources and sinks are of the order of 1 GTC (1 GTC = 10^{15} gC). Such error bars do not reflect potential systematic errors arising from our estimates of the isotopic disequilibria between the atmosphere and the oceans and biosphere, which are estimated in a separate sensitivity analysis. With respect to global totals for 1992 we found that 3.1 GTC of carbon dissolved into the ocean and that 1.5 GTC were sequestered by land ecosystems. Northern hemisphere ocean gyres north of 15°N absorbed 2.7 GTC. The equatorial oceans between 10°S and 10°N were a net source to the atmosphere of 0.9 GTC. We obtained a sink of 1.6 GTC in southern ocean gyres south of 20°S, although the deconvolution is poorly constrained by sparse data coverage at high southern latitudes. The seasonal uptake of CO_2 in northern gyres appears to be correlated with a bloom of phytoplankton in surface waters. On land, northern temperate and boreal ecosystems between 35°N and 65°N were found to be a major sink of CO_2 in 1992, as large as 3.5 GTC. Northern tropical ecosystems (equator–30°N) appear to be a net source to the atmosphere of 2 GTC which could reflect biomass burning. A small sink, 0.3 GTC, was inferred for southern tropical ecosystems (30°S–equator).

1. Introduction

Over the past two centuries, anthropogenic emissions of CO_2 by fossil fuel burning, changes in land use, and biomass burning have increased the concentration of this gas in the atmosphere by approximately 80 ppm. However, this increased CO_2 burden represents only about 50% of the cumulative loading due to fossil fuels alone. This demonstrates that strong natural sinks are currently absorbing atmospheric CO_2 at the surface of the Earth. Both the oceans and the terrestrial ecosystems can absorb CO_2 and store large quantities of carbon on this timescale. The ocean dissolves CO_2 through air-sea exchange processes and stores it in deep waters. Terrestrial ecosystems can store carbon if plant photosynthesis exceeds the release to the atmosphere by respiration. The long-term storage of carbon in an ecosystem requires mechanisms causing net ecosystem production (NEP) to be positive. Any favorable change in the availability of resources to plants such as CO_2, water, and nutrients may temporarily enhance NEP, but the long-term implications of such changes are not easy to estimate. Thus far, it has been hard to assess whether the global terrestrial biosphere has acted as a net source or as a net sink

[1]University of Colorado, Institute of Arctic and Alpine Research, Boulder.
[2]NOAA Climate Monitoring and Diagnostics Laboratory, Boulder, Colorado.
[3]National Center for Atmospheric Research, Boulder, Colorado.
[4]Department of Geological Sciences, University of Colorado, Boulder.
[5]CSIRO, Division of Atmospheric Research, Victoria, Australia.
[6]Department of Plant Biology, Carnegie Institution of Washington, Stanford, California.
[7]Department of Atmospheric Sciences, Colorado State University, Fort Collins.
[8]NASA Goddard Space Flight Center, Greenbelt, Maryland.

of atmospheric CO_2. Whether anthropogenic carbon dioxide ends up being stored in the biosphere on land, or in the oceans, has important implications for future levels of atmospheric CO_2. Storage predominantly in the ocean would be much "safer" for humanity because, in that case, CO_2 is not likely to reenter the atmosphere soon. Carbon stored in the wood and soils of terrestrial ecosystems is likely to be more temporary and also more vulnerable to continued human intervention as well as to global climate change.

Modeling the net uptake of atmospheric CO_2 by the world ocean is difficult because one has to fully account for physical circulation, chemistry, and biological processes [Maier-Reimer and Hasselmann, 1987]. Modeling the role of terrestrial ecosystems in the carbon cycle may be even more complex, given the current lack of information on different key mechanisms that interact on various scales in time and space, [e.g., Norby et al., 1992; Reynolds et al., 1992]. For both the ocean and the biosphere on land, the annual net uptake that models must estimate represents only a few percent of the one-way gross fluxes involved of CO_2 between the reservoirs of carbon.

Potentially, the isotope ratio $^{13}C/^{12}C$ of atmospheric CO_2 makes it possible to determine the global partitioning of CO_2 between ocean and land. This is because plant photosynthesis discriminates against ^{13}C, whereas the dissolution of CO_2 in the ocean proceeds with only a small fractionation. As a result, plant tissues are isotopically depleted in ^{13}C compared to the atmosphere, and a global net storage in ecosystems translates into an isotopic enrichment of the atmosphere. One of the major difficulties arising in the use of ^{13}C to study the global carbon budget is that the imprint on the atmosphere is very small. For example, variation of $\sim0.025‰$ (see note on conventions below) in the annual mean atmospheric $\delta^{13}C$ corresponds to a global net terrestrial transfer of ~1 GTC. This small change is comparable to the analytical precision ($\pm0.03‰$) for the $\delta^{13}C$ measurements made at the Institute of Arctic and Alpine Research (INSTAAR) and used in this study (M. Trolier et al., manuscript in preparation, 1994). As we are confronted with the detection of a small signal, it is helpful to have a large number of $\delta^{13}C$ measurements in the atmosphere to maximize the constraints on our diagnosis of carbon sinks.

We describe in this paper a new inverse isotopic method for calculating the intensity and the ocean/land partitioning of the CO_2 fluxes as a function of latitude and time. The inverse calculation is based on measurements of the mixing ratio and $\delta^{13}C$ of CO_2 in air samples from around the globe, provided by the Cooperative Air Sampling Network operated by the Carbon Cycle Group of the National Oceanic and Atmospheric Administration/Climate Monitoring and Diagnostics Laboratory (NOAA/CMDL). Measurements of $\delta^{13}C$ in atmospheric CO_2 from the NOAA/CMDL samples began in 1990 as a joint program between INSTAAR at the University of Colorado and NOAA/CMDL. Gaps in this new $\delta^{13}C$ data set at high southern latitudes are filled in by measurements from CSIRO (Australia). The inversion is performed using a two-dimensional zonally averaged model of atmospheric transport [Tans et al., 1989]. Results are the surface net fluxes of CO_2 and $^{13}CO_2$, which are decomposed into fossil fuel emissions, net terrestrial exchange, and net ocean exchange. The partitioning of CO_2 between land and ocean is inferred as a function of latitude and time for the period 1990–1992. Special attention is accorded in the dis-

cussion of the results for the year 1992, during which $\delta^{13}C$ data were obtained for considerably more sites.

Notes on conventions. In this paper, sinks correspond to a negative net flux of carbon (CO_2 is removed from the atmosphere) and sources to a positive net flux (CO_2 is released to the atmosphere). The total intensity of a sink denotes the net flux of carbon integrated over the whole area where the flux is negative (e.g., the northern ocean sink is 2.7 GTC). In the discussion we also split net fluxes by broad latitude bands. The extension of a sink does not necessarily coincide with the (arbitrary) limit of a broad latitude band, so that the value proposed for a sink per latitude band differs from the total intensity of this sink (e.g., the northern oceans between 30°N and 90°N sequestered 1.4 GTC).

Isotopic ratios are expressed in per mille (‰), defined as

$$\delta^{13}C = 1000 \times \left[\frac{(^{13}C/^{12}C)_{sample} - (^{13}C/^{12}C)_{standard}}{(^{13}C/^{12}C)_{standard}} \right]$$

All isotopic values in this work are given relative to the standard PDB-CO_2.

2. Global Network of Observations

A detailed presentation of the NOAA/CMDL network data set will be given elsewhere both for $\delta^{13}C$ (M. Trolier et al., manuscript in preparation, 1994) and for CO_2 mixing ratio [Conway et al., 1994]. Air samples in 2.5 L Pyrex glass flasks are currently collected in pairs approximately weekly at each site and shipped to Boulder for analysis. Each flask is analyzed by a nondispersive IR absorption technique for CO_2 (analytical precision 0.05 ppm) and by isotope-ratio mass spectrometry for $\delta^{13}C$ (analytical precision 0.03‰). A measurement is rejected if the members of a pair differ by more than 0.5 ppm in CO_2 mixing ratio, or 0.09‰ in $\delta^{13}C$.

The mixing ratio of atmospheric CO_2 is now measured routinely at almost all land sites of the network as well as aboard three ships in the Pacific (Figure 1 and Table 1). The monitoring of $\delta^{13}C$ was started in 1990 at six land sites (SMO, CHR, KUM, MLO, NWR, BRW) and aboard two ships in the Pacific (Table 1 and Figure 1). It was extended in January 1991 to site TAP and in January 1992 to 19 additional land sites and one additional ship in the South China Sea (not used in this study). The sampling program has focused on the northern hemisphere, and no $\delta^{13}C$ analyses were made on air samples collected south of 40°S. The inverse calculation of the global carbon budget requires that the field of observations be defined everywhere in latitude. Therefore we added to our $\delta^{13}C$ data set SPO and CGO, which have been measured independently by CSIRO since 1984 [Francey, 1985; Francey et al., 1990, 1994]. The groups measuring $\delta^{13}C$ at the University of Colorado and CSIRO have separate sampling programs, and the collection of air samples, the experimental designs (with potentially important differences, for example with respect to sample drying), and the calibration procedures are entirely independent. Common sampling at BRW and MLO makes it possible to intercompare the $\delta^{13}C$ data sets (Figure 2). Despite the fact that the air is collected at different intervals, the overall agreement is quite satisfactory. We applied the same curve-fitting technique [Thoning et al., 1989] to both $\delta^{13}C$ data sets (low-pass filtered in the time domain as detailed in section 3.1) and found that the discrepancy did not exceed 0.1‰ at any time
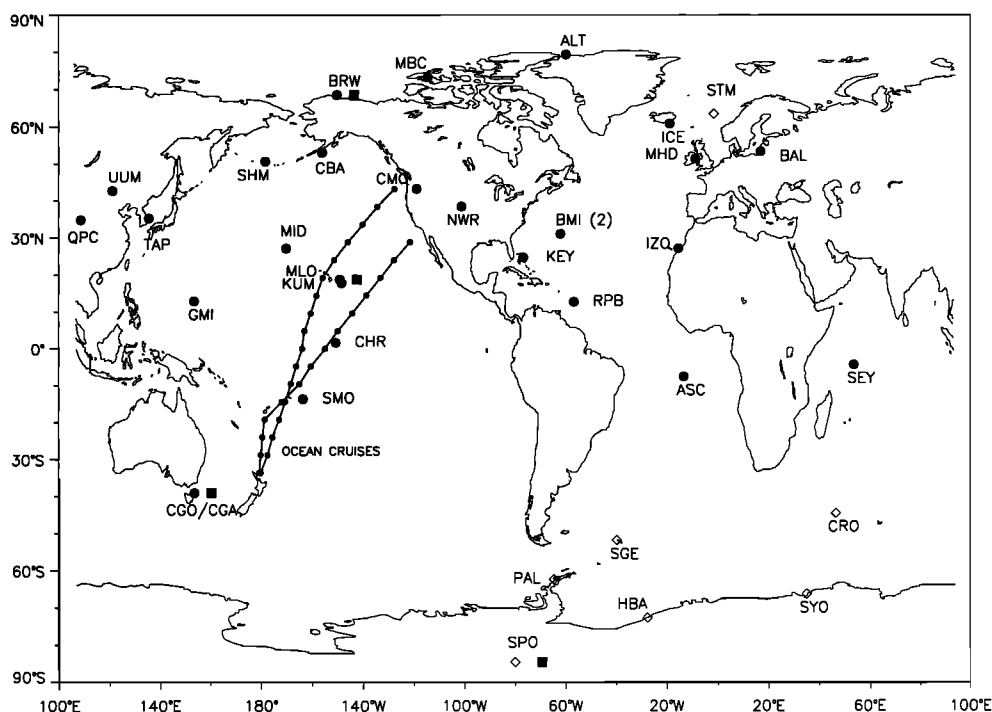
Figure 1. NOAA Climate Monitoring and Diagnostics Laboratory Cooperative Air Sampling Network in 1992. Solid circles are sites measuring CO$_2$; open circles are sites measuring δ^{13}C and δ^{18}O. CSIRO (Commonwealth Scientific and Industrial Organisation) independently measures CO$_2$, δ^{13}C, and δ^{18}O at sites we have labeled CGO, SPO, MLO and BRW.

of the period 1990–1992. Consequently, we merged δ^{13}C observations for 1992 at SPO and CGO from CSIRO with the NOAA/CMDL measurement sites without any adjustment.

3. Inverse Isotopic Model

3.1. Interpolation of Data

To perform the inverse calculation of the fields of CO$_2$ and δ^{13}C observations, we constructed a grid of the observations at regular intervals in time and latitude. This grid of observations corresponds to the grid of the two-dimensional model (see section 3.2) with 20 intervals of equal area in latitude and a time increment of 14 days. First, we smoothed the time series of flask data according to the curve fitting methods in use at NOAA/CMDL [*Thoning et al.*, 1989]. Specifically, the time series for each site was fit to a curve consisting of a polynomial trend and a sum of annual harmonics. (Flasks collected on ship tracks were regrouped into time series representing a latitude band of 5° and processed exactly as land site time series.) The interannual and short-term variability of the data was reintroduced to the fitted curve by calculating the residuals from the fit, then applying a low-pass filter in the time domain to these residuals, then adding the filtered residuals to the fitted curve. To filter the residuals in the time domain, we use a low-pass convolution filter with a full width at half maximum of 40 days for CO$_2$ and 75 days for δ^{13}C. The δ^{13}C data are smoothed more because their signal-to-noise ratio is lower. Finally, we digitized the smoothed time series of the flask data at a 14-day increment.

We then interpolated these smoothed, biweekly time series of CO$_2$ and δ^{13}C onto the model's spatial grid. To do so, we constructed a latitudinal fit of all available land and

shipboard sites every 14 days. The latitudinal fit technique is described in detail by *Tans et al.* [1989]. In this work we added a small improvement by giving a greater weight in the fit to sites where a larger number of good sample pairs are collected. Currently, δ^{13}C and CO$_2$ are weighted separately. The use of correlated weighting schemes for both species did not affect the results of the inversion. Time intervals where gaps exist in the original flask measurements were not included in the corresponding latitudinal fit. High-elevation sites (MLO, NWR, IZO) were not included in the latitudinal fit for CO$_2$.

One may anticipate that the shape of the latitudinal fit of the δ^{13}C data has an important impact on the ocean/land partitioning that is finally inferred from the inverse calculation. The sensitivity of the model to the initial fit of the observations is examined later, using a bootstrap analysis of the data. In the standard run we constrained the latitudinal fit with the largest number of sites available, independently for CO$_2$ and δ^{13}C.

3.2. Inverse Model Features

The latitudinal distribution of the surface fluxes of CO$_2$ and ^{13}CO$_2$ was inferred every 14 days from the grid of observations, using a two-dimensional model of atmospheric transport developed by *Plumb and Mahlman* [1987]. In this study, the model was run in an inverse mode, using a predictor-corrector algorithm. No interannual variability in the atmospheric transport was included. The grid of the model has 20 equal-area latitude bands (each band is 25 × 10^6 km^2 and has a specified ocean/land ratio) and 10 levels in the vertical. The time step of the model is ~8 hours, but the output is written every 14 days (the time increment of the filtered observations). The tracer ^{13}CO$_2$ was treated as a

Table 1. Atmospheric CO_2 Measurements at Network Land Sites

Code	Site	Latitude	Longitude	Elevation
SPO	south pole	89°59'S	24°48'W	2810
CGO	Cape Grim	40°41'S	144°41'E	94
S35	shipboard 35°S	≈35°S	≈175°E	0
S30	shipboard 30°S	≈30°S	≈180°W	0
S25	shipboard 25°S	≈25°S	≈180°W	0
S20	shipboard 20°S	≈20°S	≈180°W	0
S15	shipboard 15°S	≈15°S	≈175°W	0
SMO	Samoa Island	14°15'S	170°34'W	30
S10	shipboard 10°S	≈10°S	≈170°W	0
ASC	Ascension Island	7°55'S	14°25'W	54
S05	shipboard 5°S	≈5°S	≈165°W	0
SEY	Seychelles Island	4°40'S	55°10'E	3
S00	shipboard 0°N	≈0°N	≈162°W	0
CHR	Christmas Island	2°00'N	157°19'W	3
N05	shipboard 5°N	≈5°N	≈160°W	0
N10	shipboard 10°N	≈10°N	≈155°W	0
RPB	Barbados	13°10'N	59°26'W	3
N15	shipboard 15°N	≈15°N	150°W	0
GMI	Guam Island	13°26'N	144°47'E	2
KUM	Cape Kumukahi	19°31'N	154°49'W	3
MLO	Mauna Loa	19°32'N	155°35'W	3399
N20	shipboard 20°N	≈20°N	≈145°W	0
KEY	Key Biscayne	24°40'N	80°12'W	3
N25	shipboard 25°N	≈25°N	≈140°W	0
MID	Midway Island	28°13'N	177°22'W	4
IZO	Tenerife Island	28°18'N	16°29'W	2300
N30	shipboard 30°N	≈30°N	≈135°W	0
BME	Bermuda (East)	32°22'N	64°39'W	30
BMW	Bermuda (West)	32°16'N	65°53'W	30
QPC	Qinghai Province	36°16'N	100°55'E	3810
NWR	Niwot Ridge	40°03'N	105°38'W	3749
TAP	Tae-ahn Peninsula	36°44'N	126°08'E	20
CMO	Cape Meares	45°29'N	124°00'W	30
SHM	Shemya Island	52°43'N	174°06'E	40
MHT	Mace Head	53°26'N	9°44'W	5
CBA	Cold Bay	55°12'N	162°43'W	25
BRW	Point Barrow	71°19'N	156°36'W	11
MBC	Mould Bay	76°14'N	119°20'W	15
ALT	Alert	82°27'N	62°31'W	210

separate species from total CO_2 ($^{12}CO_2$ plus $^{13}CO_2$). The accuracy of our calculations of the surface fluxes depends obviously on the quality of the transport model. The largest-scale aspects of the model transport have been validated using the tracers ^{85}Kr and F-11. The vertical mixing in the lowest two layers of the model may have been underestimated in the original version [*Plumb and Mahlman*, 1987]. In this study we have set 8 m² s⁻¹ as the lowest possible value for the vertical diffusivity in the lowest layer and likewise 6 m² s⁻¹ as the lowest value for the next vertical layer (A. Plumb, personal communication, 1989). This modification improves the agreement between the simulated vertical structure of the CO_2 seasonality and the aircraft observations. A few other minor modifications in the transport have also been made.

4. Description of the Isotopic Method

The model outputs are the net surface fluxes, in GTC yr⁻¹ (1 GTC = 10^{15} gC), of CO_2 and $^{13}CO_2$ deduced from the biweekly interpolated observations, as functions of latitude (x) and time (t). The net surface flux of CO_2 is referred to as S(x, t) and the flux of $^{13}CO_2$ as ^{13}S(x, t). The inverse calculation derives S(x, t) using only CO_2 mixing ratio data, whereas ^{13}S(x, t) requires both mixing ratio and isotopic data. The decomposition of S and ^{13}S into fossil fuel emissions (S$_f$ and ^{13}S$_f$), net terrestrial exchange (S$_b$ and ^{13}S$_b$), and net ocean exchange (S$_o$ and ^{13}S$_o$) is expressed by (1) and (2). The fossil fuel component is examined in section 4.1, the terrestrial term in section 4.2, and the ocean term in section 4.3.

$$S = S_f + S_b + S_o \qquad (1)$$

$$^{13}S = {}^{13}S_f + {}^{13}S_b + {}^{13}S_o \qquad (2)$$

4.1. Fossil Fuels

Emissions of fossil CO_2 in the atmosphere (S$_f$) are prescribed in the model from monthly fuel consumption data of industrialized countries [*Marland et al.*, 1985; *Rotty*, 1986; *Andres et al.*, 1993]. The estimated accuracy of the S$_f$ is approximately 10%, which makes it the best known flux in the global carbon cycle. For 1990, 1991, and 1992 we used fossil emissions of 6.00, 6.07, and 6.10 GTC, respectively. Emissions of fossil $^{13}CO_2$ (^{13}S$_f$) in the atmosphere are expressed as follows:

$$^{13}S_f = R_f S_f \qquad (3)$$

We prescribed in the model the ^{13}C/^{12}C ratio of fossil fuels (R_f) according to *Andres et al.* [1993]. Each different source
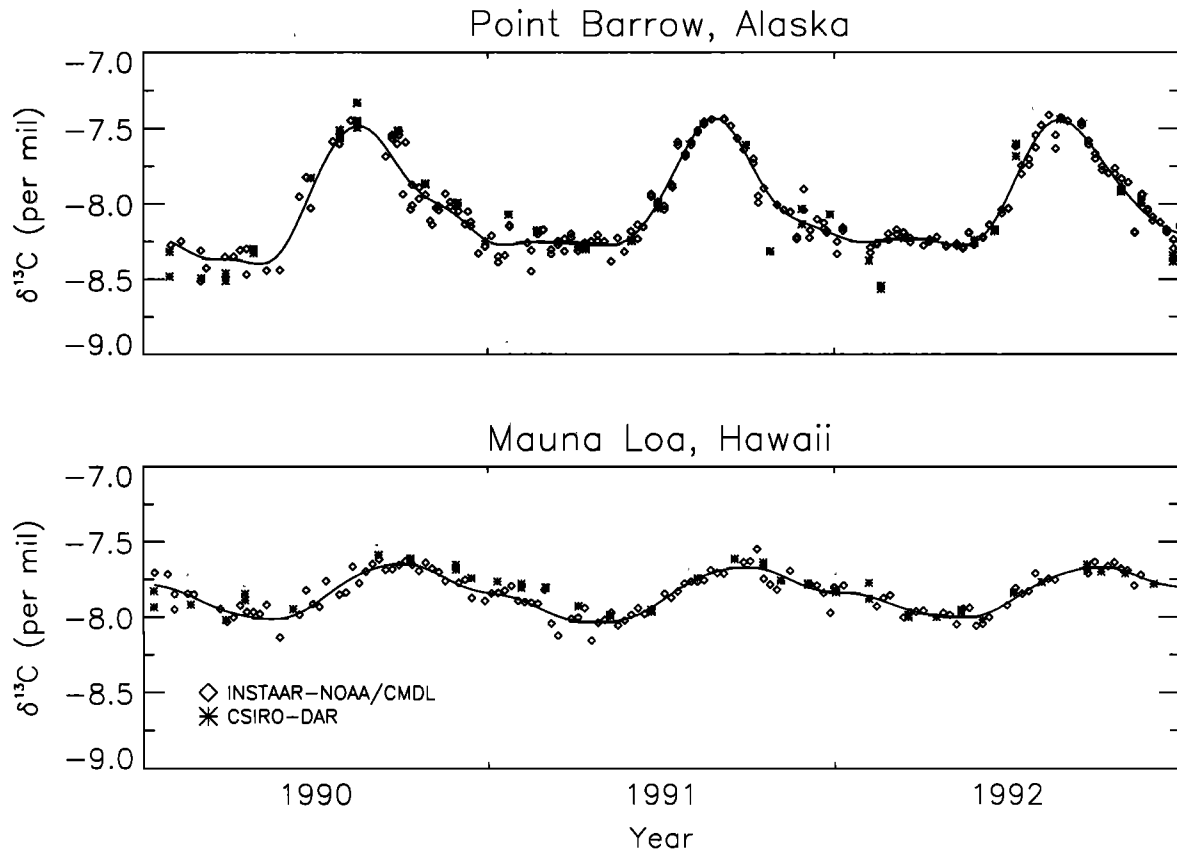
Figure 2. Comparison of $\delta^{13}C$ measurements on air samples independently collected and analyzed by the Institute of Arctic and Alpine Research, University of Colorado (pluses) and CSIRO (diamonds). The curve is a fit to the data of the same type that we used in the deconvolution for every site.

of fossil CO_2 is treated separately (oil, coal, natural gas, flaring and cement production). The $^{13}C/^{12}C$ composition of oil, related to the region of production, ranges from $-30‰$ to $-26‰$; flaring products average around $-40‰$. The $^{13}C/^{12}C$ composition of CO_2 from the burning of natural gas ($-44‰$) integrates both biogenic and thermogenic natural gas. Fossil CO_2 released by cement factories ($0‰$) and coal burning ($-24.1‰$) bears an isotopic signature largely independent of its geographical origin. The mean value of R_f in the period 1990–1992 is $-28.4‰$ [*Andres et al.*, 1993], significantly lighter than the commonly used value of $-27.4‰$ [*Tans*, 1981].

4.2. Terrestrial ^{13}C Exchange

Locally, the net flux of ^{13}C between the atmosphere and the terrestrial biosphere is the sum of two one-way fluxes, the photosynthetic uptake and the respiratory release. Plant photosynthesis stores carbon from today's atmosphere, but respiration releases carbon that has been locked up for some period of time in plant tissues and soil organic matter. Because the average $\delta^{13}C$ of the atmosphere has been decreasing since the industrial revolution, "old" biospheric carbon that is respired today is enriched in ^{13}C compared to carbon that is incorporated into the biosphere today, depending on its residence time in the terrestrial biosphere. Therefore even if the sum of biospheric uptake and release of CO_2 is near zero, the sum of the ^{13}C fluxes associated with photosynthesis and respiration is positive to the atmosphere.

We call this net isotopic enrichment of the atmosphere the "respiration isotopic disequilibrium." The CO_2 respired by plants (from aboveground material and roots) bears the same $^{13}C/^{12}C$ ratio as recent photosynthates, so the fraction of CO_2 that is cycled rapidly between atmosphere and plants has no impact on the annual mean atmospheric $\delta^{13}C$. "Older" CO_2, respired by soil heterotrophic processes, is not in isotopic equilibrium with the atmosphere. This latter flux we define as S_{resp}; it is nearly equal to the uptake (S_{ph}) associated with net primary productivity (NPP), integrated over a full year. The net exchange of CO_2 and $^{13}CO_2$ between the atmosphere and the terrestrial biosphere is given by

$$S_b = -S_{ph} + S_{resp} \qquad (4)$$

$$^{13}S_b = -^{13}S_{ph} + ^{13}S_{resp} = -\alpha_{ph}S_{ph}R_a + \alpha_{ba}S_{resp}R_b \qquad (5)$$

where α_{ph} is the fractionation associated with plant photosynthesis (see section 4.2.3; the tissues of C3 plant are depleted by about $17‰$ relative to the atmosphere and those of C-4 plants by about $4‰$); and α_{ba} is the (negligible) fractionation associated with the respiration of CO_2 by heterotrophic processes ($\alpha_{ba} = 1$).

4.2.1. Soil respiration disequilibrium. We rewrite (4) and (5) in order to make the isotopic disequilibrium of soil respiration appear explicitly, analogous to the air-sea exchange isotopic disequilibrium [*Tans*, 1980]. We define R_{ae}^b
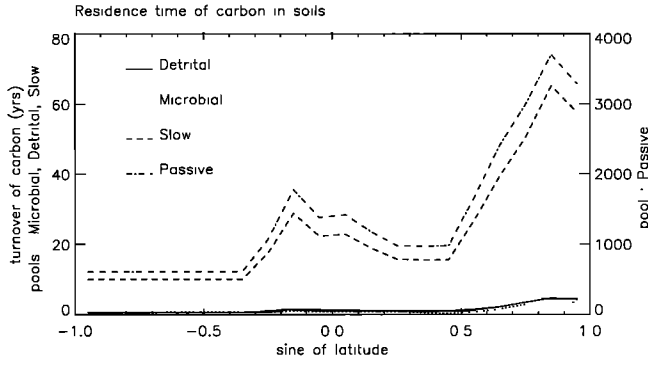
Figure 3. Turnover of soil carbon as a function of latitude from global runs of the CENTURY soil model. Detrital and microbial soil carbon turns over in less than 10 years. Slow soil carbon turns over in about 100 years and passive soil carbon (right axis) in more than 1000 years.

as the $^{13}C/^{12}C$ ratio of the atmosphere that would be in isotopic equilibrium with the biosphere [*Enting et al.*, 1993, 1994; *Tans et al.*, 1993].

$$R_{ae}^b = \frac{R_b}{\alpha_{ph}} \qquad (6)$$

Replacing (4) and (6) into (5) we obtain

$$^{13}S_b = \alpha_{ph}S_bR_a + \alpha_{ph}S_{resp}(R_{ae}^b - R_a) \qquad (7)$$

The heterotrophic respiration of CO_2 by soils is then partitioned into N_{pools}, pools of soil carbon with different turnover times (τ_i). Each pool accounts for a fraction (x_i) of the total respiration flux:

$$S_{resp} = \sum_{i=1}^{N_{pools}} {}^iS_{resp} \text{ with } {}^iS_{resp} = x_iS_{resp} \qquad (8)$$

Each pool of soil carbon retains an isotopic signature that reflects the isotopic composition of atmospheric CO_2 when it was originally photosynthesized. It is released to the atmosphere with a $^{13}C/^{12}C$ ratio $^iR_{ae}^b$, which is the isotopic ratio of the atmosphere at the time of photosynthesis, multiplied by α_{ph}.

$$^iR_{ae}^b = R_a(t - \tau_i) \qquad (9)$$

Replacing (8) and (9) into (7) we obtain

$$^{13}S_b = \alpha_{ph}S_bR_a + \alpha_{ph}S_{resp} \sum_{i=1}^{N_{pool}} x_i[R_a(t - \tau_i) - R_a(t)]$$

$$= {}^{13}S_{beq} + {}^{13}S_{bdis} \qquad (10)$$

Formally, (10) separates the net flux of ^{13}C between the atmosphere and the terrestrial biosphere into an "isoequilibrium" flux ($^{13}S_{beq}$), which has the same isotopic signature as recent photosynthates and is proportional to the net flux from the biosphere, and an isodisequilibrium flux ($^{13}S_{bdis}$) which differs from zero because the CO_2 respired by soil bears an isotopic signature lagged by τ_i relative to recent photosynthates.

A further complication arises in forest ecosystems where

we also have to account for the residence time of carbon in the aboveground biota prior to its delivery to the soil pool. We assume that metabolic material (leaves, stems) comprises 70% of the litterfall, whereas structural material (fallen branches, logs) comprises 30% [*O'Neill and De Angelis*, 1981]. A turnover time of 50 years for forest structural carbon and 1 year for metabolic carbon yields an average turnover time of 16 years in the aboveground biota which adds to the turnover time in soils. Considering the nonlinear decrease in atmospheric $\delta^{13}C$ since 1900 [*Leuenberger et al.*, 1992; R. J. Francey, personal communication, 1994], this makes the $\delta^{13}C$ of litter in forests 0.12‰ higher than today's atmosphere.

It is now well established that soil organic matter is comprised of fractions with multiple turnover times [*Harrison et al.*, 1993; *Parton et al.*, 1987; *Schimel*, 1986]. The CENTURY ecosystem model [*Schimel et al.*, 1994] uses four separate pools of carbon corresponding to detrital, microbial, slow, and passive carbon, respectively, in soils. Detrital and microbial pools consist of metabolic and structural carbon compounds rapidly decomposed and recycled to the atmosphere in less than 10 years. The slow carbon pool consists of more resistant compounds, with a high lignin content, that turn over in 10 to 100 years. The passive carbon pool turns over in more than 1000 years. *Schimel et al.* [1994] demonstrated that the turnover time of each pool is controlled by temperature and soil texture (Figure 3).

On the basis of the turnover time of carbon in soils and the residence time of carbon in the aboveground biota, we deduced the $\delta^{13}C$ of soil-respired CO_2 by using the record of atmospheric $\delta^{13}C$ from measurements over the last decades [*Keeling et al.*, 1989a] and by using ice-core data for earlier times [*Leuenberger et al.*, 1992]. An additional complication in determining the exact $\delta^{13}C$ of litter arises from the fact that plants build their tissues during the growing season, when $\delta^{13}C$ in the atmosphere is generally highest. We overcome this problem by replacing in equation (9) the latitudinal value of R_a as deduced from the 1992 observations, but weighted according to the seasonal flux of NPP [*Fung et al.*, 1987]. Historical changes in the latitudinal gradient of $\delta^{13}C$ in the atmosphere have been neglected. Figure 4 shows our estimate of $\delta^{13}C_{ae}$ of CO_2 respired by each soil carbon pool, accounting for all the complications outlined above.

Finally, we obtained the disequilibrium flux by using the total heterotrophic respiration flux (S_{resp}) from *Fung et al.* [1987] and the photosynthetic fractionation α_{ph} as detailed in 4.2.3. The soil respiration is distributed (fractions x_i) among the different pools of soil carbon according to *Schimel et al.* [1994]. Table 2 below shows that the fractions x_i do not exhibit large differences among the world biomes.

In summary, fast soil carbon (detrital and microbial pools) makes up about 80% of the heterotrophic soil respiration but has a small isodisequilibrium (less than +0.5‰). Slow soil carbon makes up about 20% of the heterotrophic respiration and can be up to +1‰ in disequilibrium. Passive soil carbon bears the isotopic signature of preindustrial photosynthates (disequilibrium equal to +1.5‰), but its contribution to the heterotrophic respiration is negligible. Generally, the disequilibrium of soil carbon increases with latitude in both hemispheres. In forest ecosystems the aging of structural plant tissues in the aboveground biota adds an additional disequilibrium to all pools of soil carbon of approximately
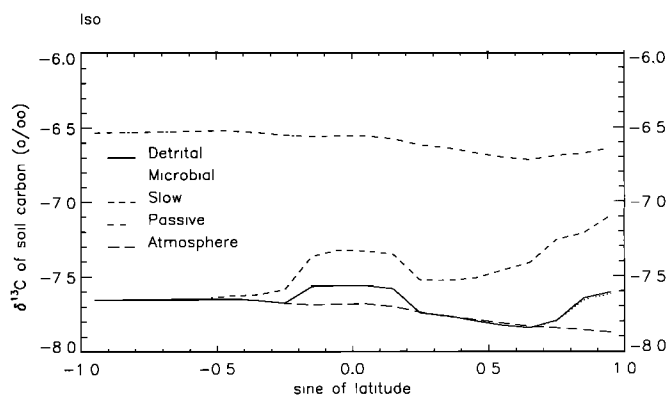
Figure 4. Disequilibrium of carbon respired by soils as a function of latitude compared to δ^{13}C of the atmosphere in 1992. The δ^{13}C disequilibrium of soil carbon is calculated from the specific turnover time of carbon in soils and in aboveground biota for forest ecosystems. The δ^{13}C of photosynthates is obtained by applying the discrimination by plants to the δ^{13}C of the atmosphere during the growing season.

Figure 5. Discrimination against ^{13}C by plant photosynthesis (Δ) as a function of latitude. Values at high-latitude areas with no plants are extrapolated. The thick continuous line is the annual mean Δ inferred from global runs of the SiB model. In the two-dimensional inverse model, 12 different monthly maps of Δ are used; the thin line plots the average "growing season" Δ, mean from June to August. The dashed line is the annual mean Δ obtained independently by *Lloyd and Farquhar* [1994].

0.12‰. Moreover, as the ^{13}C in plant tissues reflects the atmospheric δ^{13}C during the growing season, a difference of about 0.2‰ relative to the annual mean atmosphere has to be considered at high northern latitudes. The sensitivity of the model to the respiration isodisequilibrium is examined in section 5.1.1.
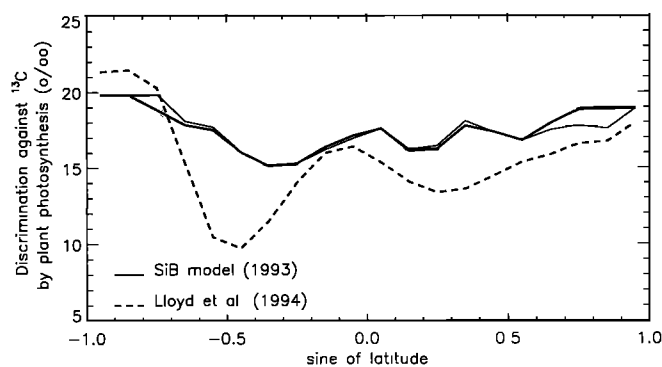
4.2.2. Biospheric destruction disequilibrium. The destruction of standing biomass in the tropics releases to the atmosphere carbon that has been stored in plant tissues for several years. Assuming that wood represents 60% of the aboveground biomass in tropical forests and that the average turnover time of carbon in the wood of tropical trees (τ_{wt}) is 50 years, we obtain a disequilibrium of approximately 0.7‰ [after *Leuenberger et al.* 1992] for CO$_2$ released by burning or deforestation in tropical forests. We assume that CO$_2$ released by the frequent burning of tropical savannas is in isotopic equilibrium with the atmosphere. The biospheric destruction disequilibrium is expressed using (11).

$$^{13}S_{des\ dis} = \alpha_{ph}S_{des}(R_a(t - \tau_{wt}) - R_a) \qquad (11)$$

In (11) the flux of CO$_2$ to the atmosphere due to biomass destruction in the tropics (S$_{des}$) is taken from the global estimates of *Houghton et al.* [1987]. Note that we have not prescribed the gross biomass destruction in our deconvolution; the net biomass destruction (forest burning minus regrowth) is a component of the total biospheric flux which is an output of the deconvolution. Provided that S$_{des}$ does not exceed 2–3 GTC (S$_{resp}$ is ~30 GTC in the northern hemisphere [*Schlesinger*, 1992]), the biospheric destruction disequilibrium in the tropics is about 10 times smaller that

Table 2. Distribution of Total Heterotrophic Respiration Among Different Pools of Soil Carbon (Fraction of Total Flux S$_{resp}$)

	Detrital	Microbial	Slow	Passive
Grasslands	0.50	0.30	0.20	<0.004
Forests	0.35	0.35	0.30	<0.004

the respiration disequilibrium at northern middle and high latitudes. Equation (11) should therefore be considered as a correction to the disequilibrium expressed by (10).

4.2.3. Discrimination against ^{13}C by plant photosynthesis. The assimilation of carbon by plants discriminates against ^{13}C because of the enzymatic preference for ^{12}C during the carboxylation reaction and because ^{13}CO$_2$ diffuses more slowly than ^{12}CO$_2$ into the stomatal cavity. The discrimination associated with the C-4 photosynthesis pathway is about 4‰ relative to the atmosphere [*Farquhar et al.*, 1989]. According to *Farquhar et al.* [1982, 1988] the discrimination (Δ) associated with photosynthesis by C-3 plants is described by

$$\Delta = 4.4 + (27.5 - 4.4)\frac{C_i}{C_a} \qquad (12)$$

where C$_a$ is the concentration of CO$_2$ in the atmosphere, and C$_i$ is the CO$_2$ concentration in the stomatal cavity. The photosynthetic fractionation factor (α_{ph}) is given by

$$\alpha_{ph} = 1 - \frac{\Delta}{1000} \qquad (13)$$

We derived monthly zonal averages of α_{ph} using the values of C$_i$ calculated by the global biosphere model SiB [*Sellers et al.*, 1986, 1988]. The SiB model is currently coupled with a general circulation model of the atmosphere and it fully accounts in a mechanistic manner for the interaction of plants with climate on a global scale, both for water and carbon [*Sellers et al.*, 1992]. The value of C$_i$ is calculated from the carbon fluxes and stomatal opening at each time step of the model according to the algorithms developed by *Collatz et al.* [1991]. The SiB model has 11 different biomes, including three types of C-4 dominated biomes in the subtropics. We assigned to C-4 dominated biomes (mostly subtropical grasslands) an overall discrimination of 15‰ to account for patches of C-3 shrubs and trees. Figure 5 plots the annual mean zonally averaged discrimination by plants as inferred from the SiB model. Larger discriminations, in the range 19–22‰, occur in temperate
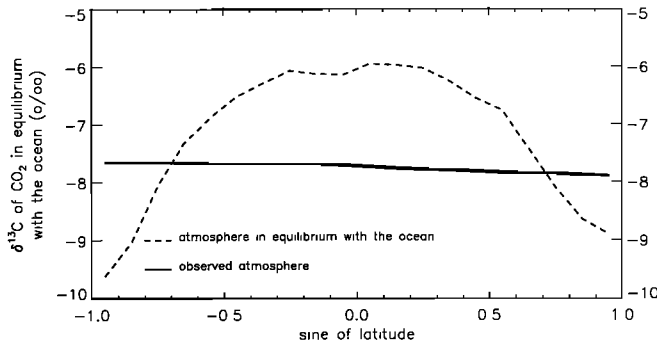
Figure 6. Ocean disequilibrium as a function of latitude. Dashed line is the $\delta^{13}C$ of the (hypothetical) atmosphere that would be in isotopic equilibrium with the ocean. The continuous line is the $\delta^{13}C$ of the actual annual mean atmosphere in 1992 from the network observations. If the $\delta^{13}C$ of the atmosphere in equilibrium with the ocean lies above the $\delta^{13}C$ of the actual atmosphere, there is an outgassing of $^{13}CO_2$ from the ocean, resulting into a net isotopic enrichment of the atmosphere.

regions of both hemispheres. Lower discriminations are encountered in tropical regions corresponding to C-4 grasslands. The "growing season" discrimination (mean from June to August) is more relevant, because it corresponds to the period of assimilation of CO_2 by plants. In temperate and boreal ecosystems where the assimilation is strongly seasonal, the growing season discrimination is on average lower than the annual mean by about 1‰ (Figure 5).

Parallel to the SiB model, we have used another field of global isotope discrimination where C_i is derived in an empirical manner from a worldwide regression of physiological data [*Farquhar et al.*, 1993; *Lloyd and Farquhar*, 1994]. The largest discrepancy between SiB and *Lloyd and Farquhar* [1994] is found in regions where C-4 plants dominate (Figure 5). Especially at around 35°S, *Lloyd and Farquhar* [1994] find a zonally averaged discrimination of 10‰, whereas SiB predicts 18‰. In C-3 dominated biomes, the SiB discrimination is systematically larger than *Lloyd and Farquhar* [1994] (Figure 5), which may be due to the fact that the mesophyll resistance of plants is neglected in SiB (approximating pCO_2 in the chloroplast by pCO_2 in the stomatal cavity). However, during the growing season, both estimates differ by 2-3‰ only. As an example, in temperate forests the discrimination estimated by *Lloyd and Farquhar* [1994] is 16-17‰ and the value from SiB is 19-20‰. Both models predict a slight increase in the discrimination of C-3 plants when going from low to high latitudes, a pattern observed by *Körner et al.* [1991] for plants growing at high altitude but not for lowland plants. The sensitivity of the inverse model to the discrimination by plants is examined in section 5.1.2.

4.3. Ocean ^{13}C Exchange

In a manner similar to (4) and (5) for the biosphere we express the net CO_2 and $^{13}CO_2$ fluxes between atmosphere and ocean using the notations of *Tans et al.* [1993].

$$S_o = -F_{ao} + F_{oa} \tag{14}$$

$$^{13}S_o = -\alpha_{ao}F_{ao}R_a + \alpha_{oa}F_{oa}R_o \tag{15}$$

where F_{ao} (F_{oa}) is one-way flux of CO_2 from (to) the atmosphere; R_o is $^{13}C/^{12}C$ ratio of ocean-dissolved inorganic carbon (DIC); α_{ao} is atmosphere $\Rightarrow$ ocean fractionation of $^{13}CO_2$ (kinetic); and α_{oa} is ocean $\Rightarrow$ atmosphere fractionation of $^{13}CO_2$ (equilibrium and kinetic). Substituting (14) into (15) and defining R_{ae}^o to be the $^{13}C/^{12}C$ isotope ratio of the atmosphere in isotopic equilibrium with the ocean,

$$R_{ae}^o = \frac{\alpha_{oa}R_o}{\alpha_{ao}}, \tag{16}$$

we obtain

$$^{13}S_o = \alpha_{ao}S_oR_a + \alpha_{ao}F_{oa}(R_{ae}^o - R_a) = {}^{13}S_{oeq} + {}^{13}S_{odis} \tag{17}$$

Similar to (10) for the biosphere, (17) separates the air-sea exchange of ^{13}C into an "equilibrium" flux ($^{13}S_{oeq}$) associated with a net transfer of carbon and a flux ($^{13}S_{odis}$) associated with the isotopic disequilibrium. The flux $^{13}S_{oeq}$ bears practically the same isotopic signature as the atmosphere because the fractionation α_{ao} associated with dissolution of CO_2 in the ocean is very small (2‰). The flux $^{13}S_{odis}$ is proportional to the disequilibrium between the atmosphere and the ocean ($R_{ae}^o - R_a$). Figure 6 plots R_a and the zonally averaged values of R_{ae}^o, as defined in (16), and shows that the ocean disequilibrium is approximately 2-3‰. Physically, R_{ae}^o differs from R_a because the atmosphere mixes $^{13}CO_2$ much faster than it can be transferred from the ocean by air-sea exchange processes. The disequilibrium flux $^{13}S_{odis}$ is controlled by the temperature dependence of the fractionation factor α_{oa} and by the field of R_o in the ocean. From Figure 6 it can be seen that $^{13}S_{odis}$ is positive to the atmosphere (atmospheric enrichment) from the equator up to approximately 60° of latitude and negative beyond (atmosphere depletion).

To obtain the isotopic disequilibrium flux $^{13}S_{odis}$, we modeled the one-way flux of CO_2 at the ocean surface (F_{oa}) as the product of an air-sea gas transfer coefficient (which depends on seasonally varying wind speeds [*Tans et al.*, 1990]), and global measurements of ΔpCO_2 from *Takahashi et al.* [1986]. The total one-way flux F_{oa} obtained in this manner is equal to 85 GTC yr^{-1}. We used the parameterization of α_{oa} derived by *Tans et al.* [1993] from separate laboratory determinations of the ^{13}C fractionation among HCO_3^-, CO_3^{2-}, and atmospheric CO_2, respectively [*Lesniak and Sakai*, 1989; *Mook et al.*, 1974]. This is expressed by (18) and (19).

$$\alpha_{oa} = 1 + \frac{\varepsilon_{oa}}{1000} \tag{18}$$

where

$$\varepsilon_{oa} = k_0 + k_1(T + k_2)T^2 \tag{19}$$

T is the sea surface temperature in degrees Celsius; $k_0 = -10.66$; $k_1 = +0.1196$; and $k_2 = -3.095 \times 10^{-4}$.

We estimated the zonally averaged distribution of R_o in the world ocean from measurements on ship cruises compiled by *Tans et al.* [1993]. The data are from *Geochemical Ocean Sections Study* [1987], *Kroopnick* [1980, 1985], and *Quay et al.* [1992]. Considering the progressive invasion of the ocean by isotopically depleted CO_2 [*Quay et al.*, 1992],

one must be careful in merging R_o measurements of water samples collected in different years. We inferred the distribution of R_o for the period 1990–1992 from the distribution in 1980 adjusted by a decreasing trend of $-0.01‰$ yr^{-1}. Another complication concerns the seasonal variations in R_o controlled by marine biological activity, the rate of upwelling of nutrient-rich, ^{13}C depleted deep waters, and to a lesser extent by air-sea exchange (a very slow process). We derived a rough order of magnitude value of the summer enrichment in ^{13}C of surface waters due to phytoplankton productivity alone as follows: Removing from 55% of the world surface waters (1000 GTC with an average winter δ^{13}C of $+1.5‰$) a fraction 75% of the global new production (15 GTC with an average δ^{13}C of $-20‰$) [*Berger et al.*, 1989; *Tans et al.*, 1993], we obtain a summer R_o value of about 2‰, thus enriched by 0.5‰ compared to the winter. However, in this study we assumed that the slow kinetics of the air-sea exchange of ^{13}CO$_2$ prevents such a seasonal signal in R_o from entering the atmosphere. The disequilibrium flux was therefore prescribed by using the annual mean values of R_o. The sensitivity of the inverse model to the ocean isotopic disequilibrium is discussed in section 5.1.2.

4.3. Partitioning CO$_2$ Between Ocean and Land Ecosystems

To infer the partitioning of CO$_2$ between ocean and land, we want to calculate the fluxes S_o and S_b in the set of equations (1) and (2). Replacing ^{13}S$_f$ using (3), and ^{13}S$_b$ and ^{13}S$_o$ with (10) and (17), in the set of equations (1) and (2) yields a simple linear system (20) for S_o and S_b, which we can solve for each latitude and time.

$$\begin{pmatrix} 1 & 1 \\ \alpha_{ao}R_a & \alpha_{ph}R_a \end{pmatrix} \begin{pmatrix} S_o \\ S_b \end{pmatrix}$$

$$= \begin{pmatrix} S - S_f \\ ^{13}S - S_f R_f - {}^{13}S_{bdis} - {}^{13}S_{defdis} - {}^{13}S_{odis} \end{pmatrix} \qquad (20)$$

The solutions are

$$S_b =$$

$$\frac{\alpha_{ao}R_a S + (R_f - \alpha_{ao}R_a)S_f - {}^{13}S + {}^{13}S_{bdis} + {}^{13}S_{odis} + {}^{13}S_{defdis}}{(\alpha_{ao} - \alpha_{ph})R_a} \qquad (21)$$

$$S_o =$$

$$-\frac{\alpha_{ph}R_a S + (R_f - \alpha_{ph}R_a)S_f - {}^{13}S + {}^{13}S_{bdis} + {}^{13}S_{odis} + {}^{13}S_{defdis}}{(\alpha_{ao} - \alpha_{ph})R_a} \qquad (22)$$

Note that S_o and S_b are functions of the surface fluxes (S and ^{13}S) derived from the inverse atmospheric transport model and depend only on a limited set of parameters: the fractionation factors α_{ph} and α_{ao} and the isotopic disequilibria S_{odis}, S_{bdis}, and $S_{def\,dis}$. The sensitivity of the model to the discrimination by plants and to the disequilibria is examined in the next section. We did not investigate in detail the sensitivity to the fossil fuel terms, which are supposed to be accurate to 10%. Our approach requires no "missing sink" to balance the global carbon budget as it inverts the observations directly. The sum of S_o and S_b always equals the
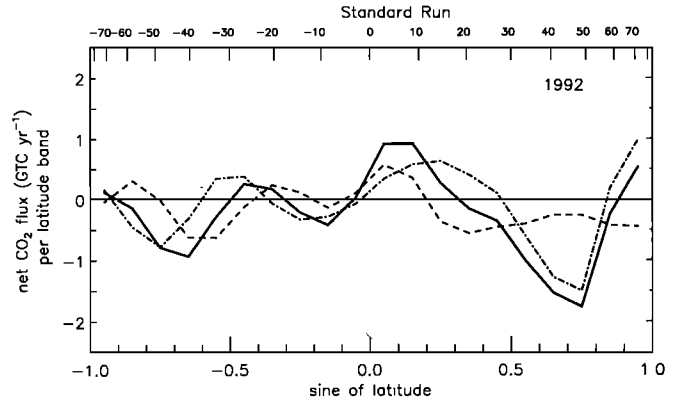
Figure 7. Latitudinal ocean/land partitioning of the sources and sinks of CO$_2$ versus latitude in the standard run of the deconvolution. Units are GTC yr^{-1} per latitude band of the model (20 bands total). The continuous line is the net flux of CO$_2$ after removal of fossil fuels. The dashed line is the net flux of CO$_2$ exchanged with the oceans. The dashed-dotted line is the net flux exchanged with land ecosystems. The sum of ocean and land fluxes equals the total net flux of CO$_2$.

total net flux S, which is inferred from the inversion of the CO$_2$ mixing ratio data alone. If, for example, the δ^{13}C data "force" the model to overestimate the flux into the ocean at a given latitude, it will be at the expense of the flux into the terrestrial biosphere.

5. Results and Sensitivity Study

In the standard run of the model, all sites available are used to constrain the inversion, all disequilibria are prescribed as detailed above, and the discrimination of ^{13}C by plants is from the SiB model. The model is initialized in a 5-year run using δ^{13}C data measured by CSIRO since 1985 at SPO, CGO, MLO, and BRW [*Francey et al.*, 1990] and the corresponding CO$_2$ data at these sites from NOAA/CMDL [*Conway et al.*, 1994]. Figure 7 plots the annual mean latitudinal pattern of the CO$_2$ sources and sinks. Units for net fluxes in Figure 7 are GTC yr^{-1} per latitude band of the model. Figure 8 plots the seasonality in the tropics. Figure 9 plots the seasonality in the northern hemisphere and Figure 10 for the Arctic. We first examine the sensitivity of the model in section 5.1 in order to estimate errors associated with the ocean/land partitioning. We then discuss the latitudinal patterns in section 6.1, the seasonality in section 6.2, and the global patterns in section 6.3.

5.1. Sensitivity Study

5.1.1. Sensitivity to the biospheric disequilibria. We compared the standard run with a run in which the biospheric disequilibrium is set to zero (experiment 1). Figure 11 plots the latitudinal pattern of the CO$_2$ sources and sinks in this experiment. Experiment 1 underscores the importance of the biospheric disequilibrium in forest ecosystems. Compared to the run with no disequilibrium, the standard run has a smaller terrestrial uptake in the northern hemisphere as well as in the southern tropics. In the northern hemisphere this is because both the turnover of soil carbon is long (Figure 3) and the release of CO$_2$ from the soils is important during the summer [*Fung et al.*, 1987]. On land
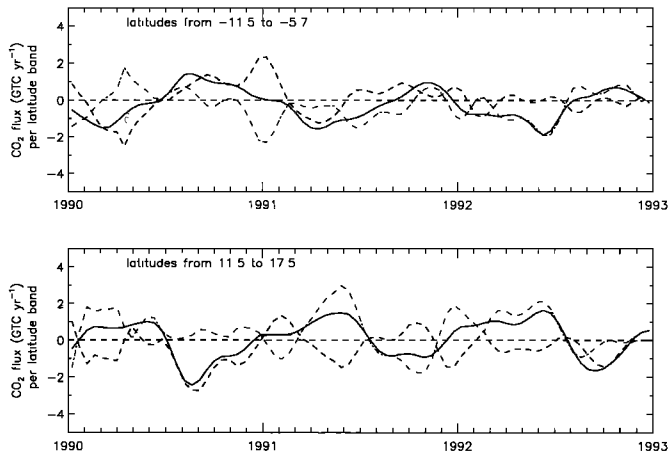
Figure 8. Seasonal ocean/land partitioning of the sources and sinks in the tropics for the standard run of the deconvolution; same legend as in Figure 7. The absence of structure in the land/ocean partitioning for years 1990 and 1991 is due to the lack of data to constrain the inversion.

this results in a northern hemisphere terrestrial sink in the standard run which is lower by 0.7 GTC compared to the run with no disequilibrium (Figure 11). At the same time, the biospheric disequilibrium makes the net ocean uptake stronger by 0.7 GTC in the northern hemisphere. Figure 11 shows that the ocean gyres are a small sink of CO$_2$ between 40°N and 60°N, whereas their uptake would be zero with no biospheric disequilibrium. In the tropics the disequilibrium occurs because of the residence time of carbon in the aboveground biota (tree wood). On land this results in a smaller sink of CO$_2$ in the southern tropics (0.5 GTC less than with no disequilibrium) and into a larger source in the northern tropics (by 0.25 GTC). In the ocean this results in a weaker equatorial source (0.4 GTC less than with no disequilibrium). The biomass destruction disequilibrium in the tropics has almost no influence in the partitioning of CO$_2$ inferred by the model (it reduces the total terrestrial uptake in the southern tropics by less than 0.1 GTC). Assuming that our estimate of the biospheric disequilibrium is accurate to

about 30%, we derived errors for the inferred ocean/land partitioning (Table 3).

5.1.2. Sensitivity to the discrimination by plants. We compared in experiment 2 the standard run of the model (discrimination from the SiB model) with a run where we use the discriminations of *Lloyd and Farquhar* [1994]. The results of experiment 2 are plotted in Figure 12. The discrimination of *Lloyd and Farquhar* [1994] yields a significant source of CO$_2$ on land between 40°S and 30°S (about 1 GTC larger than when the SiB discrimination is used), a pattern due to the large proportion of C-4 assumed by *Lloyd and Farquhar* [1994] for this latitude band. Our present knowledge of the carbon fluxes associated to biospheric destruction does not validate this terrestrial source in the southern hemisphere, although we must note that our measurement sites in this latitude band are distant from the continents. The discrimination of *Lloyd and Farquhar* [1994] makes the terrestrial source in the northern tropics larger by about 0.9 GTC than when we use the SiB value. Finally, the uptake on land in the band 30°N to 60°N is stronger by 0.8 GTC when using *Lloyd and Farquhar* [1994] compared to SiB. In this case, the ocean becomes a net source of CO$_2$ to the atmosphere between 40°N and 50°N.

It is difficult to model the discrimination by plants at the ecosystem level, and hence on a global scale, with precision better than 1–2‰. The results of experiment 2 show that the strength of the northern terrestrial sink ranges from 4 GTC to 4.6 GTC for two different modeled discriminations. Furthermore, as the discrimination by plants is strongly related to carbon assimilation and water stress, it may vary from year to year. Changes in the value of discrimination due to the interannual variability of climate (induced by the Pinatubo eruption in 1991 or the ENSO anomaly in 1991–1992) may impact the δ^{13}C in the atmosphere. Assuming the disequilibria to be more or less constant from one year to the next, such fluctuations in the discrimination add a small uncertainty in the estimate of the global mean partitioning of CO$_2$ between ocean and land. This effect should be small, because the time series of δ^{13}C in the atmosphere do not show year-to-year changes in the amplitude of the seasonal cycle of δ^{13}C larger than a few hundredths per mille [*Keeling et*
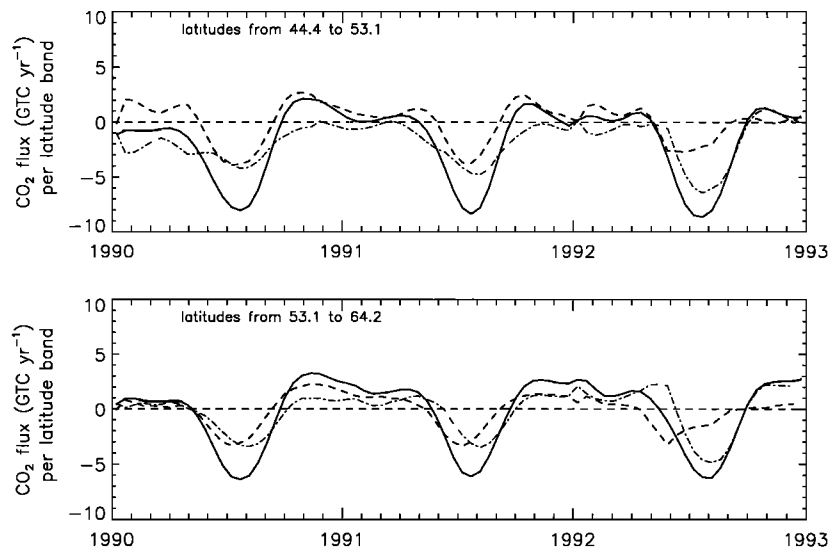
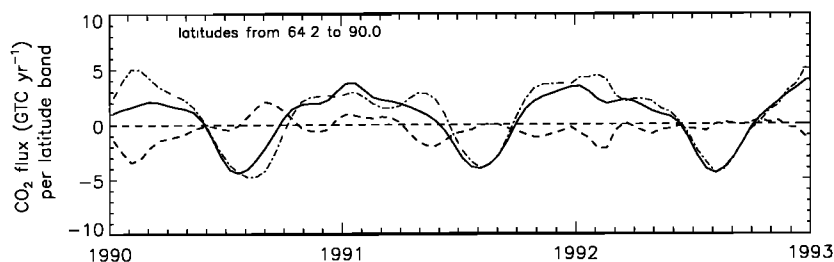**Figure 9.** Same as Figure 8 but for northern middle and high latitudes.

Figure 10. Same as Figure 8 but for the Arctic.

al., 1989a], which could correspond with year-to-year changes in the discrimination of 0.5–1‰.

We make a very coarse estimate of the uncertainty associated with the discrimination. Based on the experimental measurement of $\delta^{13}C$ in a large number of plant species [Troughton, 1972; Körner et al., 1991] it is reasonable to take for the discrimination of C-3 ecosystems a 1σ error of 1‰. This is supported by the fact that SiB (growing season) and Lloyd and Farquhar [1994] are within a range of 2–3‰ for C-3 ecosystems. Because the differences between SiB and Lloyd and Farquhar [1994] demonstrate that a large uncertainty in the estimate of the zonally averaged discrimination is due to the proportion of C-4 plants, we assumed a 1σ error on the discrimination of 3‰ at latitudes corresponding to tropical grasslands. Table 4 presents the corresponding uncertainty in the ocean/land partitioning as inferred by the inverse model. We note that the error on the estimate of the discrimination has a limited impact on the inferred partitioning.

5.1.3. Sensitivity to the ocean disequilibrium. We compared the standard run of the model with a run in which the ocean disequilibrium is set to zero (experiment 3). The results of experiment 3 as a function of latitude are plotted in Figure 13. The ocean disequilibrium has a large influence on the partitioning of the CO$_2$ inferred by the model between latitudes 30°S and 30°N. Assuming no ocean disequilibrium, the model infers an oceanic source at equatorial and southern tropical latitudes and enhances the terrestrial uptake in the tropics. This is because the ocean disequilibrium, positive at latitudes lower than 60°, tends to increase the $\delta^{13}C$ in the atmosphere, which in turn reduces the strength of the terrestrial uptake inferred by the model. (At high latitudes, north of 60°N, the ocean disequilibrium is negative and the

situation is reversed.) At northern midlatitudes this effect is diminished by the smaller area of ocean. Figure 13 shows that the ocean disequilibrium does not greatly affect the inferred terrestrial sink in the northern hemisphere. In the southern ocean, Figure 13 shows that the partitioning of CO$_2$ calculated by the model is fairly sensitive to the ocean disequilibrium. An underestimate of the ocean disequilibrium (air-sea gas transfer coefficient or $^{13}C/^{12}C$ of dissolved inorganic carbon (DIC) in surface waters) would then contribute to the (unrealistic) terrestrial sink inferred at around 50°S, to be discussed in section 6.1.1. Assuming that the uncertainty in our estimate of the ocean disequilibrium is about 30%, we derived errors (Table 5) for the inferred ocean/land partitioning.

5.1.4. Sensitivity to the isotopic composition of fossil fuels. We compared the standard run of the model with a run in which the $\delta^{13}C$ of fossil fuels is set to −27‰ instead of −28.4‰ (experiment 4). The results of experiment 4 plotted in Figure 14 show that this parameter of the model has only a small impact on the inferred land/ocean partitioning. Using −27‰ instead of −28.4‰ reduces the northern hemisphere terrestrial uptake by 0.3 GTC.

5.2. Sensitivity of the Inverse Method to the Selection of Measurement Sites

5.2.1. Increasing the number of measurement sites from 1990 to 1992. We conducted a sensitivity test (experiment 5) in which only the sites measured in 1990 were used in 1992 to infer the global carbon budget. When all 1992 sites were used, we found that the net terrestrial sink in the northern hemisphere (30°–60°N) was stronger by 1.5 GTC. The phasing of the ocean and terrestrial uptake for experiment 5 is plotted in Figure 15 for those latitudes. In the standard run, the terrestrial uptake of CO$_2$ in summer is much larger than in experiment 5. We also found that in the standard run, the seasonal ocean uptake occurs 1 or 2 months sooner and is very rapid in the spring, underscoring its possible connection with a bloom in phytoplankton productivity. Figure 15 illustrates that significant differences in the patterns of the inferred CO$_2$ fluxes arise from the introduction of more sites in the inversion, which underscores the importance of the density of measurements in this type of study. Changes in the partitioning of CO$_2$ from 1991 to 1992, especially in the
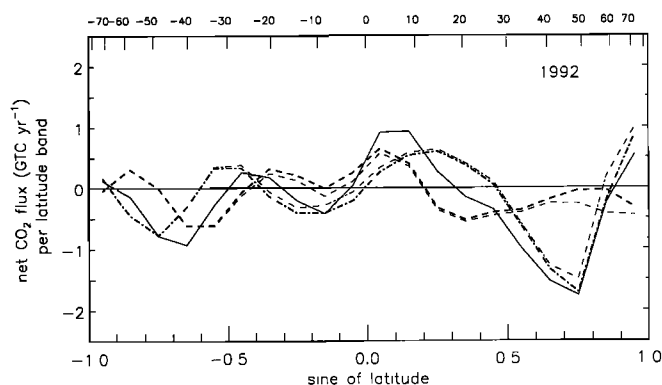
Figure 11. Latitudinal ocean/land partitioning of the sources and sinks of CO$_2$ versus latitude. Comparison of the standard run (thin lines) with a run where the biosphere isotopic disequilibrium is set to zero (thick lines).

Table 3. Errors Associated With Uncertainty in Estimate of Biospheric Disequilibrium

Latitude	90°S–30°S	30°S–Equator	Equator–30°N	30°N–90°N
Error (GTC yr^{-1})	—	0.1	<0.1	0.2
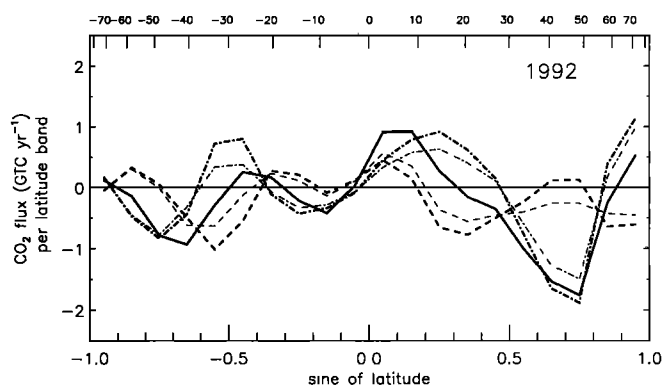
Figure 12. Latitudinal ocean/land partitioning of the sources and sinks of CO_2 versus latitude. Units are GTC yr^{-1} per latitude band of the model (20 bands total). Comparison of the partitioning between ocean and land for two different scenarios of the discrimination against ^{13}C by plant photosynthesis (Figure 6). The thick line is for the discrimination from *Lloyd and Farquhar* [1994]. The thin line is for the discrimination of the SiB model (standard run).

northern hemisphere, are largely the result of adding more sites in the inversion rather than true interannual variability of the carbon cycle (see Figures 8 and 9). A simple correction for this bias is proposed in section 6.3.

5.2.2. Bootstrap analysis and longitudinal variability. We performed a bootstrap analysis on the sites used to constrain the inversion. The bootstrap technique selects sites at random among the 38 available in the 1992 data set to construct the meridional gradient of $\delta^{13}C$ in the atmosphere. One site can be picked multiple times by the bootstrap sampling, in which case the position of each clone is slightly offset in latitude. Latitudinal curves fitted to each bootstrap selection of sites were then digitized onto the model grid, and the inverse deconvolution applied to them. In the southern hemisphere where few sites are available, the bootstrap selection was forced to pick SPO, CGO, and SMO at least once to enable the construction of the full meridional gradient. At high northern latitudes the bootstrap was forced to pick CBA or BRW or ALT at least once. Site TAP clearly bears the isotopic signature of fossil fuel (3.5 to 4.5 ppm higher in CO_2 and 0.25‰ lower in $\delta^{13}C$ than other sites at similar latitudes) because of its proximity to an industrialized area. We allowed TAP in the bootstrap selection although its weight was decreased. With bootstrap selections containing TAP, the model can explore configurations corresponding to longitudes where the air is significantly influenced by fossil fuels (Europe, North America). We ran 20 different bootstrap inversions, which makes it possible to estimate a 1σ standard deviation of the net ocean and terrestrial sources and sinks of CO_2 by broad latitude bands. A bootstrap selection picks the same set of sites for both ^{13}C and CO_2. This is necessary because we do not want to assign the $\delta^{13}C$

Table 4. Errors Associated With Uncertainty in Estimate of Discrimination

Latitude	90°S–30°S	30°S–Equator	Equator–30°N	30°N–90°N
Error (GTC yr^{-1})	<0.1	0.1	0.1	0.2
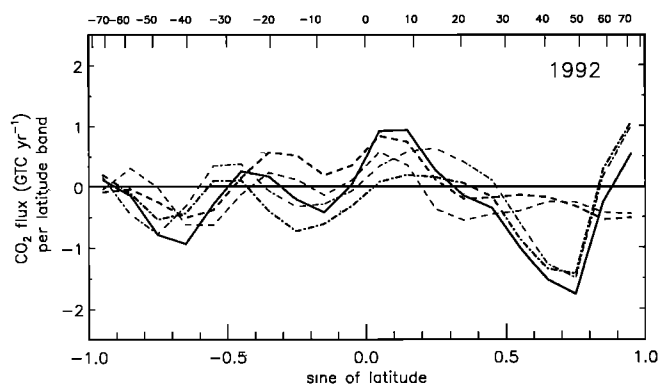
Figure 13. Latitudinal ocean/land partitioning of the sources and sinks of CO_2 versus latitude. Units are GTC yr^{-1} per latitude band of the model (20 bands total). Comparison of a run where the ocean isotopic disequilibrium is set to zero (thick lines) with the standard run (thin lines).

of one site to the CO_2 concentration of another site at the same latitude. Table 6 gives errors estimated from the bootstrap analysis for the surface flux of CO_2 (S), the surface flux of $^{13}CO_2$ (^{13}S), and for the ocean/land partitioning. The variance in the partitioning between land and oceans is due to variance in both S and ^{13}S. The variance of the partitioning is not a simple sum of the variances of S and ^{13}S because the deviations of S and ^{13}S for any individual bootstrap selection are highly correlated.

6. Results and Discussion

6.1. Latitudinal Patterns

6.1.1. Southern Ocean. Figure 7 shows a large sink of CO_2 between 30°S and 60°S which must be in the southern ocean. At high southern latitudes the CO_2 inversion is constrained by six sites, but the $\delta^{13}C$ inversion is constrained only by CGO and SPO (Figure 1). The interpolated meridional gradient of $\delta^{13}C$ is arbitrarily assumed to be flat between CGO and SPO, which biases the determination of the CO_2 partitioning between ocean and land. This may cause the appearance of the unrealistically large terrestrial sink south of CGO in Figure 7. Recent shipboard measurements of $\delta^{13}C$ in both the surface ocean and the atmosphere (R. J. Francey and H. Beggs, personal communication, 1994) suggest that there is a trough in atmospheric $\delta^{13}C$ around 55°S, which would diminish the terrestrial sink that we obtain at high southern latitudes. In addition, a wrong estimate of the ocean disequilibrium at high southern lati-

Table 5. Errors Associated With Uncertainty in Estimate of Ocean Disequilibrium

Latitude	90°S–30°S	30°S–Equator	Equator–30°N	30°N–90°N
Error (GTC yr^{-1})	0.4	0.4	0.4	<0.1

Two different types of errors are folded into this table: the uncertainty of the $\delta^{13}C$ values of dissolved inorganic carbon (DIC) in surface waters due to the sparseness of the measurement and the uncertainty of the equilibrium isotopic fractionation factor between atmospheric CO_2 and DIC. The uncertainty of the latter quantity is as large as 0.2‰ [*Tans et al.*, 1993] and dominates the error on the global scale, which could be as large as 1 GTC.

tudes, where few measurements of R_O are available, could also contribute to the unrealistic terrestrial nature of the CO_2 sink south to 40°S. Finally, it is important to note that the terrestrial sink at 50°S is correlated to the nearby terrestrial source inferred at around 30°S. In the inverse model, an incorrect estimate of [13]S at any one latitude always has an effect on inferred sources and sinks in neighboring latitudes. To avoid the problems caused by the artificial terrestrial sink at 50°S, we estimate the total partitioning in the entire zone south of 20°S, for which we obtain an uptake of 1.6 ± 1 GTC into the ocean and −0.2 ± 1 GTC on land.

6.1.2. Equatorial and tropical regions: Ocean. Figure 7 shows that the ocean is a net source of CO_2 to the atmosphere in the equatorial regions between 10°S and 10°N. This release is largely due to the outgassing of waters supersaturated in CO_2 which upwell in the tropical Atlantic and Pacific Oceans [*Andrie et al.*, 1986; *Feely et al.*, 1994]. In 1992 our model calculations suggest a net source of 0.9 ± 1.3 GTC for the equatorial oceans, which is at the lower end of previous estimates. As an example, *Heimann and Keeling* [1989] calculated a net equatorial ocean source of 1.3 GTC (their ocean source F_{EQU} and uniform ocean sink F_{UOS} between 12°S and 12°N). *Tans et al.* [1990] calculated a net equatorial ocean source of 1.3 GTC between 15°N and 15°S, based on measurements of pCO_2 in surface waters with an air-sea gas exchange consistent with the global ocean ^{14}C inventory. In 1992 the equatorial ocean source inferred by our model is displaced to the north of the equator, whereas the existing ΔpCO_2 data sets suggest that the maximum should be at the equator or shifted slightly to the south. It is possible that an anomalous pattern of equatorial upwelling prevailed during 1992 [*Francey et al.*, 1994]. As relatively few sites are available to constrain the inversion in the band 10°S–10°N (Table 1), this hypothesis remains to be confirmed.

However, 1992 was an anomalous year with respect to global temperature and the El Niño Southern Oscillation (ENSO) phenomenon (discussion in section 6.3). The low estimate we obtain for 1992, compared to the other estimates of the equatorial ocean source averaged over longer terms, may suggest that the upwelling in the tropical oceans was reduced by the weak ENSO which developed in 1991–1992.

Land: Figure 7 shows that land ecosystems are a weak sink of atmospheric CO_2 in the southern tropics (−0.3 ± 1.0
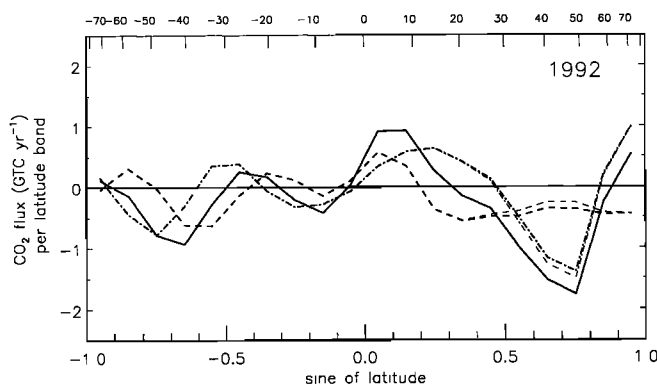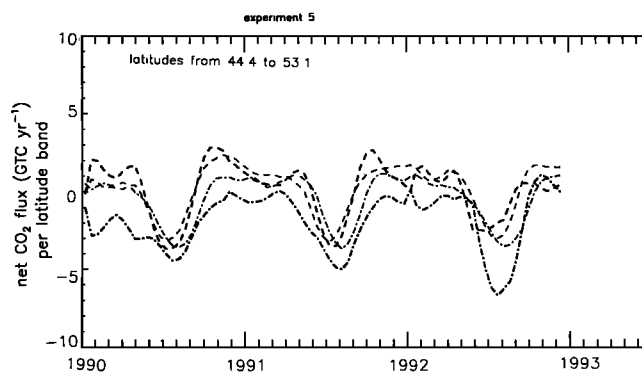
Figure 15. Seasonal ocean/land partitioning of the sources and sinks at northern temperate latitudes. Comparison of the standard run with a run where fewer sites are used to constrain the deconvolution in 1992. The thin lines are for a run where only the sites available in 1990 have been used for 1992.

GTC) but an important source in the northern tropics (2.0 ± 1.3 GTC). The sink in the southern tropics is likely contributed by rain forest ecosystems, mostly in Amazonia and Southeast Asia, and integrates both the net release of CO_2 to the atmosphere due to deforestation and the net ecosystem production (NEP) of undisturbed and regrowing forests. If the existence of a weak terrestrial sink in the southern tropics is confirmed by further measurements, it suggests two possibilities. One possibility is that equatorial forests between 20°S and the equator are currently fertilized in such a manner that their NEP compensates entirely a local deforestation of about 0.85 GTC yr^{-1} [*Houghton et al.*, 1987]. Mechanisms that could bring about such a fertilization have not been identified with certainty, although some physiologists think it is likely that the fixation of anthropogenic nitrogen and higher temperatures could enable a CO_2 fertilization effect [*Gifford*, 1994]. Another possibility is that the destruction of forests in the southern tropics has been overestimated. This idea has been supported by recent analyses for Latin America [*Houghton et al.*, 1991; *Skole and Tucker*, 1993] which underscore the uptake of carbon by recovering forests on land abandoned by shifting agriculture and also suggests reduced clearing rates based on satellite analyses.

The northern tropics terrestrial source inferred by our model is 2.0 ± 1.3 GTC in 1992. *Houghton et al.* [1987] estimate the deforestation in the northern tropics at 0.9 GTC, which leaves ~1.1 GTC of our inferred source unexplained in 1992. The intensity of the northern tropics source inferred by the model depends on the discrimination prescribed for plants (section 5.2). However, a smaller terrestrial source would require 0°–30°N ecosystems to discriminate more than our estimated 17‰ by several per mille, an unlikely possibility because of the abundance of C-4 plants (in African savannas) in this latitude band. Another possible bias of our diagnosis is the overrepresentation of the Pacific in the NOAA/CMDL network for the northern tropics. Alternatively, if the intrahemispheric transport between the low and the temperate latitudes of the northern hemisphere is weaker in the model than in the real world, the model would infer a source of CO_2 at low latitudes that is too large. This is because the excess CO_2 from fossil fuel burning would be transported to those latitudes in the real world but

Figure 14. Latitudinal ocean/land partitioning of the sources and sinks of CO_2 versus latitude. Comparison of a run (thick lines) where $\delta^{13}C$ of fossil fuels is set to −27‰ with the standard run (thin lines) where $\delta^{13}C$ of fossil fuels is −28.4‰.

Table 6. Error Estimates (in GTC yr^{-1}) Associated With Longitudinal Variability of Data Derived From Bootstrap Analysis

Latitude	90°S–30°S	30°S–Equator	Equator–30°N	30°N–90°N	Global
S	0.5	0.6	0.6	0.5	0.2
^{13}S × 90	···	0.6	0.6	0.6	0.2
Partitioning	···	0.4	0.7	0.5	0.3

Uncertainties in the flux of ^{13}CO$_2$ (^{13}S) have been multiplied by 90 and expressed as a flux of total carbon in GTC yr^{-1} (the natural abundance of ^{13}C is ~1.11%). No error estimate is given at high southern latitudes for ^{13}S and the ocean/land partitioning because SPO and CGO were always included in the bootstrap site selections, in the absence of isotopic data from other high-latitude southern sites.

not in the model. This possibility will be resolved when more detailed calibrations of the transport via new tracers, such as SF$_6$, become available.

Recent studies agree that the burning of savannas causes a huge seasonal release of CO$_2$ to the atmosphere, up to 1.6 GTC every year [*Andreae*, 1991; *Crutzen and Andreae*, 1990; *Houghton*, 1991], about 3 times as much carbon as the release by forest burning in the tropics [*Hao et al.*, 1988, 1990]. It is not certain whether such a huge seasonal release drives a net annual release because it is followed by rapid regrowth. In the analysis of *Houghton et al.* [1991] the burning of savannas is assumed to be entirely compensated by regrowth and thus results in no net release of carbon to the atmosphere. This balance may not be exact in each year. In view of the uncertainties in assessing the exact regrowth of savannas every year, the unexplained terrestrial release of 1.1 GTC for 1992 in the north tropics could partly be due to burning that is only partially compensated by regrowth. In addition, the weak ENSO episode of the first half of 1992 could have enhanced the release of CO$_2$ by tropical ecosystems, as proposed by *Keeling et al.* [1989a], who found a larger release on land associated with the ENSO episodes of the 1980s based on CO$_2$ and δ^{13}C data. The link between ENSO events and biospheric CO$_2$ fluxes is not clearly understood but might be due to factors such as fires, or changes in NPP or respiration. *Keeling et al.* [1989a] have suggested that the weaker Asian monsoon generally associated with ENSO episodes may significantly reduce the NPP in the tropics. However *Keeling et al.* [1989a] kept the fractionation by plants (α_{ph}) constant in their analysis, whereas α_{ph} could be different in ENSO years due to disturbed climate. This may have a relatively large effect on atmospheric δ^{13}C measurements, as was shown in section 5.1.2.

6.1.3. Temperate and boreal regions: Ocean. Figure 7 shows that there is a major sink of CO$_2$ in the ocean of −2.7 ± 1.1 GTC, almost uniformly distributed between 15°N and the Arctic. The strength of this sink is 2.3 GTC larger than the northern gyres sink calculated by *Tans et al.* [1990] for the non-ENSO years of the 1980s. The spatial patterns of the ocean sink inferred by the model can be compared to pCO$_2$ measurements in surface waters, though the physics of air-sea exchange also influences the net flux of CO$_2$ at the air-sea interface. Measurements from *Inoue et al.* [1993] and *Takahashi et al.* [1986] suggest that the midlatitude Pacific gyres cannot be a very large sink of atmospheric CO$_2$. North Atlantic pCO$_2$ data reveal a deep trough between 50°N and 60°N. Tropical Atlantic data show large differences between the western and the eastern gyre regions, where the outgassing of water in upwelling regions is partly counteracted by a strong phytoplankton productivity [*Copin-Montegut and*

Avril, 1993]. The NOAA/CMDL network contains 5 sites measured for CO$_2$ and δ^{13}C in the northern Atlantic Ocean (BME, BMW, IZO, MHT, ICE) and 12 sites in the northern Pacific Ocean (GMI, MLO, KUM, SHM, MID, CBA, CMO, 5 ship sites). To check whether the standard model run was biased in favor of the Pacific gyres, we performed an experiment including only the Atlantic sites in this latitude band. This inversion yielded an ocean uptake in the northern gyres comparable to the standard run.

Land: Figure 7 shows that there is a major sink of CO$_2$ in the land biosphere between 30° and 60°N. This terrestrial sink, likely located in temperate deciduous and subboreal conifer forests, is −3.5 ± 0.9 GTC in 1992, with a maximum net uptake at around 50°N. The cause of this sink is not known. The northern hemisphere terrestrial sink inferred in this study is at the upper limit of current estimates. For example, *Tans et al.* [1990] require a terrestrial sink ranging from 2.7 ± 0.7 GTC to balance the carbon budget of the 1980s, although an enhanced terrestrial sink may have operated in the 1990s.

The potential sink on land in the northern hemisphere has also been addressed by process-based ecological models. The ideal model would have to consider the influence on plants and soils of changes in the availability of CO$_2$, water, and nutrients. For example, it is generally accepted that higher CO$_2$ concentration in the atmosphere enhances photosynthesis at the leaf level, but recent studies [*Körner and Arnone*, 1993; *Norby et al.*, 1992] have pointed out that higher CO$_2$ may also cause a reallocation of photosynthates to fine root tissues that are ultimately decomposed at the end of the growing season with no net storage of carbon. Until such mechanisms are fully understood and included in models, it is very difficult to model the NEP with the desired accuracy (smaller than 10% of the one-way fluxes). An alternative approach to estimate the terrestrial sink is to use forestry data. However, uncertainties arise in estimating the fate of carbon in soils of logged forests as well as the fate of wood products such as paper and plywood [*Harmon et al.*, 1990]. Recent compilations of forestry data [*Kauppi et al.*, 1992; *Kohlmaier et al.*, 1993; *Sampson et al.*, 1993; *Houghton*, 1993; *Sedjo*, 1992] estimate a sink of 0.7–1.2 GTC in forests of the northern hemisphere, which is ~2 GTC smaller than that found in this study. An attractive method to evaluate this sink is the direct appraisal of NEP by continuous CO$_2$ flux measurement [*Wofsy et al.*, 1993], but the extrapolation of such results to very large areas remains problematic.

6.1.4. Arctic regions (north of 65°). Figure 7 shows that in 1992 the ecosystems north of 60°N were a net source of 1 GTC, and the flux into the Arctic Ocean was −0.4 ± 1.0

GTC. Although surface temperatures have been increasing in the Arctic for the past 30 years [*Bradley et al.*, 1993], there is limited evidence for a net terrestrial release of CO_2 by local ecosystems. *Tans et al.* [1990] hypothesized an Arctic terrestrial source of 0.4 to 0.7 GTC in order to balance the global carbon budget of the 1980s. Recent flux measurements in the area of BRW suggest that Arctic tundra could be a source of 0.3 GTC [*Oechel et al.*, 1993]. Indeed, the carbon balance of Arctic peatlands appears to be very sensitive to climate change. An increase in temperature or a decrease in stored water may enhance the release of CO_2 by soils and lakes [*Billings et al.*, 1982, 1983; *Klinig et al.*, 1991] and turn Arctic biomes into a net source of CO_2. Given the large amount of carbon presently stored in Arctic soils, this mechanism may have important implications for future CO_2 levels [*Webb and Overpeck*, 1993]. However, there is probably a bias in our model due to the location of our measurement sites. North of 60°N the sites measured for $\delta^{13}C$ (BRW, CBA, MBC, ALT) are maritime sites reached by polluted continental air masses (low $\delta^{13}C$, high CO_2) transported from lower latitudes [*Conway and Steele*, 1989; *Halter and Harris*, 1983; *Halter et al.*, 1985].

Tans et al. [1989] concluded that the two-dimensional model misallocates CO_2 sources/sinks between the Arctic and the midlatitudes when it is constrained by maritime air data alone. Constraining the $\delta^{13}C$ inversion with maritime data alone may thus overestimate both the uptake of CO_2 at temperate latitudes and the release of CO_2 by Arctic lands, especially during the winter when polluted air is frequently captured in the polar boundary layer.

6.2. Seasonal Patterns

6.2.1. Tropical and equatorial regions.
Figure 8 shows the seasonality of the CO_2 fluxes in the tropics. In the northern tropics, there is a net terrestrial release of CO_2 to the atmosphere from December to July. In the southern tropics, there is a net terrestrial uptake from December to July. Figure 8 shows that in our model the seasonality of the CO_2 fluxes in the tropics is largely driven by the biosphere on land. The seasonal terrestrial source in the tropics corresponds approximately to the dry season and may be linked to the burning of savannas (mostly in Africa) during the dry season. From the inverse model we estimate the release in the northern tropics during the dry season at 1.3 ± 0.7 GTC, at the upper limit of the range given by *Crutzen and Andreae* [1990] and *Andreae* [1991] for savanna fires alone (0.3–1.7 GTC). The phasing of the terrestrial CO_2 emissions in the tropics is in agreement with the observed occurrence of African savanna fires [*Cahoon et al.*, 1992]. Fire activity diminishes in northern tropical Africa by May, when Figure 8 shows the start of a decrease in terrestrial CO_2 emissions.

6.2.2. Northern hemisphere seasonality on land.
Figures 9 and 10 plot the seasonal partitioning of CO_2 at middle and high northern latitudes. Figure 9 shows that the biosphere on land dominates the seasonal exchange of CO_2. During the growing season the uptake by plants is more pronounced at 50°N than at 60°N (Figure 9). From October to May, there is a net release of CO_2 by the ecosystems which increases northward from about zero at 50°N, to 1.8 GTC at 60°N, up to 2.6 GTC at 70°N. This pattern could be partly caused by the misallocation by the two-dimensional model discussed earlier. Although the inversion technique makes it possible to separate the biosphere on land from the ocean, it does not

allow us to distinguish between photosynthesis and respiration in net terrestrial exchange. At low latitudes it is plausible that photosynthesis is still maintained during the winter but it seems unlikely that it can compensate respiration to yield a net flux close to zero, as indicated by Figure 9. Emissions of CO may play a role in this feature. Although a full CO correction [*Enting and Mansbridge*, 1991] is beyond the scope of this paper, the assumption that 5% of fossil fuel carbon is initially released as CO would result in an enhancement of the winter terrestrial release in the temperate zone of approximately 0.3 GTC. Another possibility (see section 6.1.2) would be that the model transports excess fossil fuel CO_2 away from these regions too slowly during the winter.

Figure 9 shows that the onset of net CO_2 uptake by plants occurs in early June. There is no change in the phasing of this event with increasing latitude, as observed by *Conway et al.* [1988] from the CO_2 data alone. Another interesting feature is the brief release of CO_2 by the biosphere on land that precedes the growing-season uptake north of 50°N. Possibly, this release of 1 GTC over 4 months is associated with enhanced respiration by roots and soils due to a rise of temperature in spring, as suggested by modeling studies [*Bonan*, 1991; C. Waelbroeck, personal communication, 1994] and observations for high-latitude ecosystems [*Coyne and Kelley*, 1978].

6.2.3. Northern hemisphere seasonality in the ocean.
Figure 9 also displays the seasonality of the ocean fluxes in the northern hemisphere. The phasing of the ocean fluxes is controlled by the physics of air-sea gas transfer and by phytoplankton productivity. Figure 9 shows that the ocean absorbs CO_2 during the spring and summer. Of particular interest is the quick drawdown of CO_2 between April and May, which leads by about 2 months the maximum uptake on land (Figure 9). The inverse calculation produces this pattern because the 1992 data set contains several maritime sites (SHM, MHT, CBA) in areas where the ocean productivity increases abruptly during the spring [*Feldman et al.*, 1989].

The difference in pCO_2 between atmosphere and ocean (ΔpCO_2) can be independently derived as an output of the model from the inferred ocean flux S_o. Using the piston velocity field of *Erickson* [1993], we obtain in that manner realistic annual mean ΔpCO_2 everywhere in the ocean, which provides a good check of the validity of our calculations. The rapid spring rise in the ocean uptake followed by a slow recovery to winter conditions matches the observed seasonal trends of pCO_2 in North Atlantic surface waters [*Smith et al.*, 1991; *Watson et al.*, 1991; *Takahashi*, 1986]. However, during the spring we obtain pCO_2 values in northern gyres of the order of 200 ppm, which is much too low. This suggests that the model may overestimate the spring uptake or that the piston velocity is not correctly estimated.

6.2.4. Seasonality in Arctic regions (north of 65°).
The seasonality in the Arctic is plotted in Figure 10. The uptake of CO_2 is entirely terrestrial and lasts only from May to August. The pronounced drawdown of CO_2 obtained in May is reasonable considering that when the upper soil thaws, Arctic plants are able to sustain photosynthesis even under low light and cold temperatures [*Tieszen*, 1978]. We attempted to derive a rough estimate of the summer uptake by plants north of 65°N (14×10^6 km² total) as follows: We first extrapolated a tundra uptake of 120 gCO_2 m⁻² from May to

Table 7. Annual Mean Sources and Sinks for Broad Latitude Bands (Positive Numbers, Sources to the Atmosphere)

	90°S–Equator	Equator–30°N	30°N–65°N	65°N–90°N	Global
1992 total	−2.2	1.6	−4.5	+0.6	−4.6
Land	−0.9	2.0	−3.5	+1.0	−1.4
Ocean	−1.3	−0.4	−1.0	−0.4	−3.1
Error	±1.0	±1.3	±0.9	±1.0	±1.1
1991 total	−2.5	1.2	−3.6	+0.7	−4.2
Land	−1.1	0.9	−2.7	+1.1	−1.8
Ocean	−1.4	0.3	−0.9	−0.4	−2.4
1990 total	−1.4	+0.8	−3.3	+0.7	−3.2
Land	−0.2	+1.6	−4.9	+1.3	−2.2
Ocean	−1.2	−0.8	+1.6	−0.6	−1.0

The errors apply both to ocean and to land net fluxes; they are derived from the bootstrap analysis (Table 6) and from the uncertainty in the estimates of the disequilibria and discrimination (Tables 3, 4, 5). Errors have not been estimated for 1990 and 1991, though they will be larger than for 1992, because fewer sites were measured for $\delta^{13}C$ in the earlier years.

September [*Whiting et al.*, 1992] to a total tundra surface area of 7×10^6 km^2 and obtained 0.2 GTC. We then extrapolated an uptake of 960 gCO_2 m^{-2} [*Bonan*, 1991] from May to September to the remaining 7×10^6 km^2 of boreal forests and obtained 1.8 GTC. Altogether, this yields a total summer uptake of 2 GTC north of 65°N, in good agreement with our derived value of 2.3 ± 0.5 GTC. The model results are not so good in winter where the release of CO_2 that we found (3 ± 0.9 GTC) may be overestimated (see section 6.1.4.).

6.3. Global Totals

In this section we examine the global ocean/land partitioning inferred from the inverse model for the period 1990–1992. Estimated CO_2 land and ocean fluxes, integrated over broad latitude bands, are given in Table 7. These values represent a CO_2 flux budget, not a carbon storage budget. Our isotopic method is diagnostic of where and when CO_2 is exchanged with the land or the ocean, but it does not reveal the ultimate reservoir of storage. Every year, about 0.4 GTC of the carbon absorbed on land is transported by rivers and could end up being stored in the ocean [*Sarmiento and Sundquist*, 1992]. Also, there is no correction to the budgets in Table 7 to account for the production of CO_2 by oxidation of CO in the troposphere.

There are two components to the estimated errors in Table 7. First, there are errors derived from the bootstrap analysis. These errors are primarily random in character, although the location of the sampling sites, which overrepresent the oceans, can introduce systematic errors into the deconvolution. Second, there are errors arising from uncertainties in our estimates of plant discrimination and the biospheric and oceanic isotopic disequilibria. These latter errors tend to be systematic rather than random; if, for example, our estimate of the air-sea isotopic disequilibrium were off by 0.2‰, our partitioning of carbon sinks between oceans and land would change by ~1 GTC globally, with errors of the same sign in all latitude bands.

The values in Table 7 do not represent the true interannual variability of the ocean/land partitioning during 1990–1992, because of the effects on our deconvolution of the change in

the number of sites measured for $\delta^{13}C$ from 1990 to 1992. Recent climate anomalies induced by the Pinatubo eruption in June 1991 and the ENSO event developing in 1991–1992 certainly have perturbed the transfer of CO_2 between the atmosphere, the ocean, and the land biota. *Dutton and Christy* [1992] showed that the first half of 1992 was warmer than 1990 and 1991, at least partially because of the 1991–1992 ENSO episode. However, the second half of 1992 was colder, possibly because of scattering by the aerosols emitted from the Pinatubo eruption. In the annual mean temperature, cooling predominated and 1992 was the coldest year since 1986 [*Halpert et al.*, 1993]. To correct the results in Table 7 for the changing site densities, we have applied a "site density correction," the difference between the 1992 inversion results with all sites (standard run) and the 1992 inversion results with the 1990 sites only (experiment 5), to the 1990 and 1991 data. (A site density correction is not needed for the CO_2 fluxes because they are inferred from the CO_2 data alone, and the number of sites measured for CO_2 is nearly the same from 1990 to 1992.) The results for 1990 should be regarded with particular caution, because the band 30°–65°N was constrained for $\delta^{13}C$ only by NWR, a high-elevation site in the Colorado Rocky Mountains. The corrected CO_2 fluxes are shown in Table 8. The main effect of the site density correction is to reduce the terrestrial uptake and to enhance the ocean uptake in the band 30°–65°N by 0.7 GTC. The site density correction also reduces the terrestrial release in the Arctic by 0.3 GTC.

Table 7 shows that the global sink of CO_2 increased from 3.0 GTC in 1990 to 4.5 GTC in 1992 [see *Conway et al.*, 1994]. The largest change between 1991 and 1992 occurred in the band 30°–65°N, where the net sink of CO_2 increased by 0.9 GTC. Our deconvolution results suggest that this increase took place on land. We cannot determine whether this is due to enhanced photosynthesis or to lowered respiration in northern temperate ecosystems. Generally, the NPP of temperate ecosystems is more sensitive to precipitation than to temperature [*Dai and Fung*, 1993]. The respiration in boreal and cold-deciduous forests responds primarily to temperature [*Dai and Fung*, 1993; *Dörr and Munnich*, 1987] and could be very important in the interannual variability. The Pinatubo aerosols induced a cooling in the northern hemisphere of 0.5°–0.7°C in 1992 [*Dutton and Christy*, 1992]. Assuming that respiration is doubled for a rise in temperature of 10°C [*Raich and Schlesinger*, 1992], such a cooling would decrease the respiration in deciduous and boreal forests, which is typically ~30 GTC, by 4% [*Schlesinger*,

Table 8. Annual Mean Sources and Sinks in 1990 and 1991 for Broad Latitude Bands, Corrected for Number of Sites Used to Constrain Inversion

	90°S–Equator	Equator–30°N	30°N–65°N	65°N–90°N	Global
1991 total	−2.5	1.2	−3.6	+0.7	−4.2
	Corrected				
Land	−1.3	0.8	−2.0	+0.8	−1.7
Ocean	−1.2	0.4	−1.6	−0.1	−2.5
1990 total	−1.4	+0.8	−3.3	+0.7	−3.2
	Corrected				
Land	−0.4	+1.5	−4.2	+1.0	−2.1
Ocean	−1.0	−0.7	+0.9	−0.3	−1.1

Table 9. Comparison of Global CO_2 Budgets of 1980s With Inverse Deconvolution for 1992 [after *Tans et al.*, 1994]

	90°S–16°S	Equatorial	16°N–90°N	Global
Keeling et al				
land	−0.1	+0.3	−0.6	−0.5
ocean	−1.1	+1.1	−2.3	−2.3
fossil	+0.2	+0.2	+4.8	+5.2
Tans et al.				
land	−0.1	+0.5	−2.3	−1.9
ocean	−1.1	+1.3	−0.6	−0.4
fossil	+0.2	+0.2	+4.9	+5.3
This work				
land	−0.2	+0.8	−2.2	−1.5
ocean	−1.4	+0.7	−2.4	−3.1
fossil	+0.2	+0.3	+5.6	+6.1

We use the standard case scenario of *Keeling et al.* [1989b] for the year 1984, with a global deforestation of 1.8 GTC yr^{-1}. We use scenario 7 of *Tans et al.* [1990] for 1981–1988 with a global deforestation of 1 GTC yr^{-1}. The sums do not add up exactly due to rounding errors. "Land" denotes the sum of all fluxes on land, including the deforestation in the studies of *Keeling et al.* [1989b] and *Tans et al.* [1990].

1992]. This would enhance the annual net terrestrial uptake by ~1.2 GTC. The ongoing monitoring of $\delta^{13}C$ at all the NOAA/CMDL sites should bring more insights into such interannual patterns.

Finally, in Table 9 we compare our results (for 1992) with the global CO_2 budgets for the 1980s established by *Keeling et al.* [1989b] and *Tans et al.* [1990]. In the southern hemisphere and in equatorial regions, our results compare well both with *Keeling et al.* [1989b] and *Tans et al.* [1990]. In the northern hemisphere the region of the so-called "missing sink," we infer an ocean sink close to the value proposed by *Keeling et al.* [1989b] but also a terrestrial sink close to the value proposed by *Tans et al.* [1990]. Between the mid-1980s and 1992, substantial changes in the global carbon cycle include an increase in fossil fuel emissions by 0.7 GTC yr^{-1} and an increase in the global sink of CO_2 (ocean plus land) of 1.5 GTC, mostly located in the northern hemisphere (a model-independent feature).

7. Conclusions

We describe in this paper a new isotopic method based on the inverse deconvolution of the observed distributions of CO_2 and $\delta^{13}C$ in the atmosphere. We use a new data set of $\delta^{13}C$ measurements from NOAA/CMDL and the University of Colorado, with sample coverage expanding from 1990 to 1992 to include 25 sites and three ship tracks. Additional $\delta^{13}C$ data at high southern latitudes come from the Australian group at CSIRO. The isotopic method determines the net partitioning of CO_2 between the ocean and the terrestrial ecosystems as a function of latitude and time. Besides the ocean isotopic disequilibrium, 2 factors of importance in the $\delta^{13}C$ of the atmosphere are treated in detail. First, the isotopic disequilibrium on land is inferred from a recent global estimate of the turnover time of carbon in soils and aboveground biota. Second, the global discrimination by plants is estimated from two independent physiological models. Both factors impact the inferred uptake on land for the northern hemisphere by about 1 GTC each. The large number of measurement sites allows a bootstrap analysis of

the inversion, providing an estimate of the error of our two-dimensional calculations partially accounting for the longitudinal variability of the data.

Our results suggest that there is a major sink of −3.5 ± 1.0 GTC in temperate and boreal forests and a major ocean sink of −2.7 ± 1.1 GTC from 15° to 90°N. We find that the Arctic ecosystems north of 65°N are a net source of CO_2 of 1.0 ± 1.0 GTC, but this conclusion could be biased by the maritime characteristics of all our Arctic sites. The northern tropics are a net terrestrial source of CO_2 of 2.0 ± 1.3 GTC, whereas the southern tropics are only a weak terrestrial sink of −0.3 ± 1.0 GTC. The equatorial oceans account for an annual release of 0.9 ± 1.3 GTC. The seasonality of the CO_2 exchange in the tropics shows a large terrestrial release in the dry season, possibly linked to savannah fires. The seasonality at northern midlatitudes displays a rapid ocean uptake in spring that we attribute to a bloom of phytoplankton productivity.

In conclusion, the simple and inexpensive two-dimensional inverse isotopic model that we present in this study, used in conjunction with an extensive set of atmospheric $\delta^{13}C$ measurements, partitions CO_2 fluxes between ocean and land with some realism. This model complements the global mean partitioning provided by one-dimensional box diffusion isotopic models but also makes it possible to explore the latitudinal structure and the seasonality of the sources and sinks. A larger number of measurement sites is crucial in accurately determining the structure of the carbon cycle. The next step in the utilization of atmospheric $\delta^{13}C$ as a constraint on the partitioning of CO_2 will be a full three-dimensional analysis, which is currently under way.

References

Andreae, M. O., Biomass burning: Its history, use, and distribution and its impact on environmental quality and global climate, in *Global Biomass Burning: Atmospheric, Climatic and Biospheric Implications*, edited by J. S. Levine, MIT Press, Cambridge, Mass., 1991.

Andres, R. J., G. Marland, T. Boden, and S. Bishoff, Carbon dioxide emissions from fossil fuel combustion and cement manufacture 1751–1991 and an estimate of their isotopic composition and latitudinal distribution, in *The Carbon Cycle*, Cambridge University Press, New York, 1993.

Andrie, C., C. Oudot, C. Genthon, and L. Merlivat, CO_2 fluxes in the tropical Atlantic during FOCAL cruises, *J. Geophys. Res., 91*, 11,741–11,755, 1986.

Berger, W. H., V. S. Smetacek, and G. Wefer, Ocean productivity and paleoproductivity—An overview, in *Productivity of the*

Ocean: Present and Past, Dalhem Workshop Reports, edited by W. H. Berger et al., John Wiley, New York, 1989.

Billings, W. D., J. O. Lukem, D. A. Mortensen, and K. M. Peterson, Arctic tundra: A source or a sink for atmospheric carbon dioxide in a changing environment, *Oecologia, 53*, 7–11, 1982.

Billings, W. D., J. O. Luken, D. A. Mortensen, and K. M. Peterson, Increasing atmospheric carbon dioxide: Possible effects on Arctic tundra, *Oecologia, 58*, 286–289, 1983.

Bonan, G. B., Atmosphere-biosphere exchange of carbon dioxide in boreal forests, *J. Geophys. Res., 96*, 7301–7312, 1991.

Bradley, R. S., F. T. Keiming, and H. F. Diaz, Recent changes in the North American Arctic boundary layer in winter, *J. Geophys. Res., 98*, 8851–8858, 1993.

Cahoon, D. R., B. J. Stocks, J. S. Levine, W. R. Cofer, and K. O'Neill, Seasonal distribution of African savanna fires, *Nature, 359*, 812–815, 1992.

Collatz, G. J., J. T. Ball, C. Grivet, and J. A. Berry, Physiological and environmental regulation of stomatal conductance, photosynthesis and transpiration: A model that includes a laminar boundary layer, *Agric. For. Meteorol., 54*, 107–136, 1991.

Conway, T. J., and L. P. Steele, Carbon dioxide and methane in the Arctic atmosphere, *J. Atmos. Chem., 9*, 81–89, 1989.

Conway, T. J., P. P. Tans, L. S. Waterman, K. W. Thoning, K. A. Masarie, and R. H. Gammon, Atmospheric carbon dioxide measurements in the remote global troposphere, 1981–1984, *Tellus, 40*, 81–115, 1988.

Conway, T. J., P. P. Tans, L. S. Waterman, D. R. Kitzis, K. A. Masarie, M. Stavish, and N. Zhang, Evidence for interannual variability of the carbon cycle from the NOAA/CMDL global air sampling network, *J. Geophys. Res., 99*, 22,831–22,855, 1994.

Copin–Montegut, C., and B. Avril, Continuous pCO_2 measurements in surface waters of the northeastern tropical Atlantic, paper presented at 4th International CO_2 Conference, World Meteorol. Organ., Carqueiranne, France, 1993.

Coyne, P. I., and J. J. Kelley, Meteorological assessment of CO_2 exchange over an Alaskan Arctic tundra, in *Vegetation and Production Ecology of the Alaskan Arctic Tundra*, edited by L. L. Tieszen, Springer-Verlag, New York, 1978.

Crutzen, P. J., and M. O. Andreae, Biomass burning in the tropics: Impact on atmospheric chemistry and biogeochemical cycles, *Science, 250*, 1669–1677, 1990.

Dai, A., and I. Fung, Can climate variability contribute to the "missing" CO_2 sink?, *Global Biogeochem. Cycles, 7*, 599–609, 1993.

Dörr, H., and K. O. Munnich, Annual variation in soil respiration in selected areas of the temperate zone, *Tellus, Ser. B, 39*, 114–121, 1987.

Dutton, E. G., and J. R. Christy, Solar radiative forcing at selected locations and evidence for global lower tropospheric cooling following the eruptions of El Chichōn and Pinatubo, *Geophys. Res. Lett., 19*, 2313–2316, 1992.

Enting, I. G., and J. V. Mansbridge, Latitudinal distribution of sources and sinks of CO_2: Results of an inversion study, *Tellus, Ser. B, 43*, 156–170, 1991.

Enting, I. G., C. M. Trudinger, R. J. Francey, and H. Granek, Synthesis inversion of atmospheric CO_2 using the GISS tracer transport model, *Tech. Pap. 29*, pp. 1–44, Aust. Div. Atmos. Res., Commonwealth Sci. and Ind. Res. Organ., Melbourne, 1993.

Enting, I. G., C. M. Trudinger, and R. J. Francey, A synthesis inversion of the concentration and $\delta^{13}C$ of atmospheric CO_2, *Tellus*, in press, 1994.

Erickson, D. J., III, A stability dependent theory for air-sea gas exchange, *J. Geophys. Res., 98*, 15,669–15,678, 1993.

Farquhar, G. D., M. H. O'Leary, and J. A. Berry, On the relationship between carbon isotope discrimination and the intercellular carbon dioxide concentration in leaves, *Aust. J. Plant Physiol., 9*, 121–137, 1982.

Farquhar, G. D., K. T. Hubick, A. G. Condon, and R. A. Richards, Carbon isotope fractionation and plant water-use efficiency, in *Stable Isotopes in Ecological Research*, edited by P. W. Rundel et al., Springer-Verlag, New York, 1988.

Farquhar, G. D., J. R. Ehleringer, and K. T. Hubick, Carbon isotope discrimination and photosynthesis, *Annu. Rev. Plant Physiol., 40*, 503–537, 1989.

Farquhar, G. D., J. Lloyd, J. A. Taylor, L. B. Flanagan, J. P. Syvertsen, K. T. Hubick, S. C. Wong, and R. Ehleringer, Vegetation effects on the isotope composition of oxygen in atmospheric CO_2, *Nature, 363*, 439–443, 1993.

Feely, R. A., R. Wanninkhof, C. E. Cosca, M. J. McPhaden, R. H. Byrne, F. J. Millero, F. P. Chavez, T. Clayton, D. M. Campbell, and P. P. Murphy, The effect of tropical instability waves on CO_2 species distributions along the equator in the eastern equatorial Pacific during the 1992 ENSO event, *Geophys. Res. Lett., 21*, 277–280, 1994.

Feldman, G., et al., Ocean color, availability of the global data set, *Eos Trans. AGU, 70*, 634–635, 640–641, 1989.

Francey, R. J., Cape Grim isotope measurements—A preliminary assessment, *J. Atmos. Chem., 3*, 247–260, 1985.

Francey, R. J., F. J. Robbins, C. E. Allison, and N. G. Richards, The CSIRO global survey of CO_2 stable isotopes, in *Baseline 1988*, edited by S. R. Wilson, 1990.

Francey, R. J., C. E. Allison, I. G. Enting, J. W. C. White, M. Trolier, and P. P. Tans, Changes in the oceanic and terrestrial carbon uptake since 1982, *Nature*, in press, 1994.

Fung, I. Y., C. J. Tucker, and K. C. Prentice, Application of advanced very high resolution radiometer vegetation index to study atmosphere-biosphere exchange of CO_2, *J. Geophys. Res., 92*, 2999–3013, 1987.

Geochemical Ocean Sections Study (GEOSECS), *Atlantic, Pacific and Indian Ocean Expeditions*, vol. 7, *Shorebased Data and Graphics*, Washington, D. C., 1987.

Gifford, R. M., The global carbon cycle: A viewpoint on the missing sink, *Aust. J. Plant Physiol., 21*, 1–15, 1994.

Halpert, M. S., C. F. Ropelewski, T. R. Karl, J. K. Angell, L. L. Stowe, R. R. Heim, A. J. Miller, and D. R. Rodenhuis, 1992 brings return to moderate global temperatures, *Eos Trans. AGU, 74*, 433–438, 1993.

Halter, B., and J. M. Harris, On the variability of atmospheric carbon dioxide concentration at Barrow, Alaska during winter, *J. Geophys. Res., 88*, 6858–6864, 1983.

Halter, B. C., J. M. Harris, and K. A. Rahn, A study of winter aerosols variability in carbon dioxyde and Arctic haze aerosols at Barrow, Alaska, *Atmos. Environ., 12*, 2033–2037, 1985.

Hao, W. M., D. Scharffe, P. J. Crutzen, and E. Sanhueza, Production of N_2O, CH_4, and CO_2 from soils in the tropical savannah during the dry season, *J. Atmos. Chem., 7*, 93–105, 1988.

Hao, W. M., M. H. Liu, and P. J. Crutzen, Estimates of annual and regional release of CO_2 and other trace gases to the atmosphere from fires in the Tropics, based on the FAO statistics for the period 1975–1980, in *Fires in the Tropical Biota: Ecosystem Processes and Global Challenges, Ecol. Stud.*, vol. 84, edited by G. J. Goldammer, Springer-Verlag, New York, 1990.

Harmon, M. E., W. K. Ferrel, and J. F. Franklin, Effects on carbon storage of the conversion of old-growth forests to young forests, *Science, 247*, 699–702, 1990.

Harrison, K., W. Broecker, and G. Bonani, A strategy for estimating the impact of CO_2 fertilization on soil carbon storage, *Global Biogeochem. Cycles, 7*, 69–80, 1993.

Heimann, M., and C. D. Keeling, A three dimensional model of atmospheric CO_2 transport based on observed winds, 2, Model description and simulated tracer experiments, in *Aspects of Climate Variability in the Pacific and Western Americas, Geophys. Monogr. Ser.*, vol. 55, edited by D. H. Peterson, AGU, Washington, D. C., 1989.

Houghton, R. A., Is carbon accumulating in the northern temperate zone?, *Global Biogeochem. Cycles, 7*, 611–618, 1993.

Houghton, R. A., et al., The flux of carbon from terrestrial ecosystems to the atmosphere in 1980 due to changes in land use: Geographic distribution of the global flux, *Tellus, Ser. B, 39*, 122–139, 1987.

Houghton, R. A., D. L. Skole, and D. S. Lefkowitz, Changes in the landscape of Latin America between 1850 and 1985, II, Net release of CO_2 to the atmosphere, *For. Ecol. Manage., 38*, 173–199, 1991.

Houghton, S., Biomass burning from the perspective of the global carbon cycle, in *Global Biomass Burning: Atmospheric, Climatic and Biospheric Implications*, edited by J. S. Levine, MIT Press, Cambridge, Mass., 1991.

Inoue, H. Y., H. Matsueda, M. Ishii, K. Fushimi, and M. Hirota, Atmospheric and oceanic carbon dioxide measurements in the

western North Pacific, 1986–1992, paper presented at the 4th International CO$_2$ Conference, World Meteorol. Organ., Carqueiranne, France, 1993.

Kauppi, P. E., K. Mielikäinen, and K. Kuusela, Biomass and carbon budget of European forests, 1971 to 1992, *Science*, *256*, 70–74, 1992.

Keeling, C. D., R. B. Bacastow, A. F. Carter, S. C. Piper, T. P. Whorf, M. Heimann, W. G. Mook, and H. A. Roeloffzen, A three-dimensional model of atmospheric CO$_2$ transport based on observed winds, 1, Analysis of observational data, in *Aspects of Climate Variability in the Pacific and Western Americas*, *Geophys. Monogr. Ser.*, vol. 55, edited by D. H. Peterson, 165–236, AGU, Washington, D. C., 1989a.

Keeling, C. D., S. C. Piper, and M. Heimann, A Three-dimensional model of atmospheric CO$_2$ transport based on observed winds, 4, Mean annual gradients and interannual variations, in *Aspects of Climate Variability in the Pacific and Western Americas*, *Geophys. Monogr. Ser.*, vol. 55, edited by D. H. Peterson, pp. 305–363, AGU, Washington, D. C., 1989b.

Klinig, G. W., G. W. Kipphut, and M. C. Miller, Arctic lakes and streams as gas conduits to the atmosphere: Implications for tundra carbon budgets, *Science*, *251*, 298–301, 1991.

Kohlmaier, G. H., M. K. B. Lüdeke, C. Häger, F. Badeck, T. Lang, G. Würth, and M. Minster, Examination of the age class structures of the world's forests and their effect on the CO$_2$-source-sink problem, paper presented at the 4th International CO$_2$ Conférence, World Meteorol. Organ., Carqueiranne, France, 1993.

Körner, C., and J. A. Arnone, Responses to elevated carbon dioxide in artificial tropical ecosystems, *Science*, *257*, 1672–1674, 1993.

Körner, C., G. D. Farquhar, and S. C. Wong, Carbon isotope discrimination by plants follows latitudinal and altitudinal trends, *Oecologia*, *88, 1*, 30–36, 1991.

Kroopnick, P., The distribution of ^{13}C in the Atlantic Ocean, *Earth Planet. Sci. Lett.*, *49*, 469–484, 1980.

Kroopnick, P., Distribution of ^{13}C and ΣCO$_2$ in the world oceans, *Deep Sea Res.*, *32*, 57–77, 1985.

Lesniak, P. M., and H. Sakai, Carbon isotope fractionation between dissolved carbonate (CO$_3^{2-}$) and CO$_2$(g) at 25° and 40°C, *Earth Plan. Sci. Lett.*, *95*, 297–301, 1989.

Lloyd, J., and G. D. Farquhar, ^{13}C discrimination by the terrestrial biosphere, *Oecologia*, in press, 1994.

Leuenberger, M., U. Siegenthaler, and C. C. Langway, Carbon isotope composition of atmospheric CO$_2$ during the last ice age from an Antarctic ice core, *Nature, 357*, 1992.

Maier-Reimer, E., and K. Hasselmann, Transport and storage of CO$_2$ in the ocean—An inorganic ocean-circulation carbon cycle model, *Clim. Dyn.*, *2*, 63–90, 1987.

Marland, G., R. M. Rotty, and N. L. Treat, CO$_2$ from fossil fuel burning: Global distribution of emissions, *Tellus*, *37*, 243–258, 1985.

Mook, W. G., J. C. Bommerson, and W. H. Staverman, Carbon isotope fractionation between dissolved bicarbonate and gaseous carbon dioxide, *Earth Plan. Sci. Lett.*, *22*, 169–176, 1974.

Norby, R., C. A. Gunderson, S. D. Wullschleger, E. G. O'Neill, and M. McCracken, Productivity and compensatory responses of yellow-poplar trees in elevated CO$_2$, *Nature, 357*, 322–324, 1992.

O'Neill, R. V., and D. R. De Angelis, Comparative productivity and biomass relations of forest ecosystems, in *Dynamic Properties of Forests Ecosystems*, Cambridge University Press, New York, 1981.

Oechel, W. C., S. J. Hastings, G. Vourtilis, M. Jenkins, G. Riechers, and N. Grulke, Recent change of Arctic tundra ecosystems from a net carbon dioxide sink to source, *Nature, 361*, 520–523, 1993.

Parton, W. J., D. S. Schimel, C. V. Cole, and D. S. Ojima, Analysis of factors controlling soil organic matter levels in Great Plains grasslands, *Soil Sci. Soc. Am. J.*, *51*, 1173–1179, 1987.

Plumb, R. A., and J. D. Mahlman, The zonally averaged transport characteristics of the GFDL general circulation/transport model, *J. Atmos. Sci.*, *44*, 298–327, 1987.

Quay, P. D., B. Tilbrook, and C. S. Wong, Oceanic uptake of fossil fuel CO$_2$: Carbon-13 evidence, *Science, 256*, 74–79, 1992.

Raich, J. W., and W. H. Schlesinger, The global carbon dioxide flux in soil respiration and its relationship to vegetation and climate, *Tellus, 44*, 81–89, 1992.

Reynolds, J. F., D. W. Hilbert, J. Chen, P. C. Harley, P. R. Kemp, and P. W. Leadley, Modeling the response of plants to elevated CO$_2$ and climate change, *Rep. DOE/ER-60490T-H1*, U.S. Dep. of Energy, CO$_2$ Res. Prog., Washington, D. C., 1992.

Rotty, R. M., Estimates of seasonal variations in fossil fuel CO$_2$ emissions, *Tellus, 39*, 184–202, 1986.

Sampson, R. N., M. Apps, S. Brown, C. V. Cole, J. Downing, L. S. Heath, D. S. Ojima, T. M. Smith, A. M. Solomon, and J. Wisniewski, Workshop summary statement: Terrestrial biospheric carbon fluxes—Quantification of sinks and sources of CO$_2$, in *Terrestrial Biospheric Carbon Fluxes: Quantification of Sinks and Sources of CO$_2$*, edited by J. Wisniewski and R. N. Sampson, Kluwer Academic, Norwell, Mass., 1993.

Sarmiento, J. L., and E. T. Sundquist, Revised budget for the oceanic uptake of anthropogenic carbon dioxide, *Nature, 356*, 589–593, 1992.

Schimel, D. S., Carbon and nitrogen turnover in adjacent grassland and cropland ecosystems, *Biogeochemistry*, *6*, 239–243, 1986.

Schimel, D. S., B. H. Braswell, B. A. Holland, R. McKeown, D. S. Ojima, T. H. Painter, W. J. Parton, and A. R. Townsend, Climatic, edaphic and biotic controls over the storage and turnover of carbon in soils, *Global Biogeochem. Cycles, 8*, 279–293, 1994.

Schlesinger, W. H., *Biogeochemistry, An Analysis of Global Change*, Academic, San Diego, Calif., 1992.

Sedjo, R. A., Temperate forest ecosystems in the global carbon cycle, *Ambio, 21*, 190–194, 1992.

Sellers, P. J., Y. Mintz, Y. C. Sud, and A. Dalcher, A simple biosphere model (SiB) for use within general circulation models, *J. Atmos. Sci.*, *43*, 505–531, 1986.

Sellers, P. J., Y. Mintz, Y. C. Sud, and A. Dalcher, A brief description of the simple biosphere model (SiB), in *Physically-Based Modelling and Simulation of Climate Change*, Kluwer, Academic, Norwell, Mass., 1988.

Sellers, P. J., J. A. Berry, G. J. Collatz, C. B. Field, and F. G. Hall, Canopy reflectance, photosynthesis, and transpiration, III, A reanalysis using improved leaf models and a new canopy integration scheme, *Remote Sens. Environ.*, *42*, 187–216, 1992.

Skole, D., and C. Tucker, Tropical deforestation and habitat fragmentation in the Amazon: Satellite data from 1978 to 1988, *Science, 260*, 1905–1910, 1993.

Smith, W. O., L. A. Codispotti, D. M. Nelson, T. Manley, E. J. Buskey, H. J. Niebauer, and G. F. Cota, Importance of *Phaeocystis* blooms in the high-latitude ocean carbon cycle, *Nature, 352*, 514–516, 1991.

Takahashi, T., J. Goddard, S. Sutherland, D. W. Chipman, and C. C. Breeze, Seasonal and geographic variability of carbon dioxide sink/source in the oceanic areas, final technical report, contract MRETTA 19X-89675C, Lamont-Doherty Geol. Obs., Palisades, New York, 1986.

Tans, P., On calculating the transfer of carbon-13 in reservoir models of the carbon cycle, *Tellus, 32*, 464–469, 1980.

Tans, P., ^{13}C/^{12}C of industrial CO$_2$, in *SCOPE 16: Carbon Cycle Modeling*, edited by B. Bolin, John Wiley, New York, 1981.

Tans, P., T. J. Conway, and T. Nakazawa, Latitudinal distribution of the sources and sinks of atmospheric carbon dioxide derived from surface observations and an atmospheric transport model, *J. Geophys. Res.*, *94*, 5151–5172, 1989.

Tans, P. P., I. Y. Fung, and T. Takahashi, Observational constraints on the global atmospheric CO$_2$ budget, *Science, 247*, 1431–1438, 1990.

Tans, P. P., J. A. Berry, and R. F. Keeling, Oceanic ^{13}C data: A new window on CO$_2$ uptake by the oceans, *Global Biogeochem. Cycles, 7*, 353–368, 1993.

Tans, P. P., I. Y. Fung, and I. G. Enting, Storage versus flux budgets: The terrestrial uptake of CO$_2$ during the 1980's, in *Biotic Feedbacks in the Global Climate System: Will the Warming Feed the Warming?*, edited by G. M. Woodwell and F. T. Mackenzie, Oxford University Press, New York, in press, 1994.

Thoning, K. W., P. P. Tans, and W. D. Komhyr, Atmospheric carbon dioxide at Mauna Loa Observatory, 2, Analysis of the NOAA GMCC data, 1974, 1985, *J. Geophys. Res.*, *94*, 8549–8565, 1989.

Tieszen, L. L., Photosynthesis in the principal Barrow, Alaska, species: A summary of field and laboratory responses, in *Vege-*

tation and Production Ecology of the Alaskan Arctic Tundra, edited by L. L. Tieszen, Springer-Verlag, New York, 1978.

Troughton, J. H., Carbon isotope fractionation in plants, Proc. Conf. Radiocarbon Dating, Wellington, 8, 39–57, 1972.

Watson, A. J., C. Robinson, J. E. Robinson, P. J. Williams, and M. J. Fasham, Spatial variability in the sink for atmospheric carbon dioxide in the North Atlantic, Nature, 350, 50–53, 1991.

Webb, R. S., and J. T. Overpeck, Carbon reserves released, Nature, 361, 497–498, 1993.

Whiting, G. J., D. S. Bartlett, S. Fan, P. S. Bakwin, and S. C. Wofsy, Biosphere/atmosphere CO_2 exchange in tundra ecosystems: Community characteristics and relationships with multispectral surface reflectance, J. Geophys. Res., 97, 16,671–16,680, 1992.

Wofsy, S. C., M. L. Goulden, J. W. Munger, and S. M. Fan, Net exchange of CO_2 in a mid-latitude forest, Science, 260, 1314–1317, 1993.

A. Berry, Department of Plant Biology, Carnegie Institution of Washington, Stanford, CA 94305.

P. Ciais, LMCE CE Saclay, Batiment 709, L'Orme des Meurisieres, 91191, Gif-sur-Yvette, Cedex, France.

J. G. Collatz and P. J. Sellers, NASA Goddard Space Flight Center, Code 923, Greenbelt, MD 20771.

R. J. Francey, CSIRO, Division of Atmospheric Research, Victoria, Australia.

D. R. Randall, Department of Atmospheric Sciences, Colorado State University, Fort Collins, CO 80521.

D. S. Schimel, National Center for Atmospheric Research, Boulder, CO 80307.

P. Tans and M. Trolier, NOAA Climate Monitoring and Diagnostics Laboratory, 325 Broadway, Boulder, CO 80303.

J. W. C. White, Institute of Arctic and Alpine Research, University of Colorado, Boulder, CO 80302.